



Published in final edited form as:

J Muscle Res Cell Motil. 2007 ; 28(7-8): 371–395. doi:10.1007/s10974-008-9131-3.

Force transients and minimum cross-bridge models in muscular contraction

Masataka Kawai and

Department of Anatomy and Cell Biology, University of Iowa, Iowa City, IA 52245, USA

Herbert R. Halvorson

4661 Devonshire Rd., Detroit, MI 48224, USA

Masataka Kawai: Masataka-kawai@uiowa.edu; Herbert R. Halvorson: HHalvor135@aol.com

Abstract

Two- and three-state cross-bridge models are considered and examined with respect to their ability to predict three distinct phases of the force transients that occur in response to step change in muscle fiber length. Particular attention is paid to satisfying the Le Châtelier–Brown Principle. This analysis shows that the two-state model can account for phases 1 and 2 of a force transient, but is barely adequate to account for phase 3 (delayed force) unless a stretch results in a sudden increase in the number of cross-bridges in the detached state. The three-state model ($A \rightarrow B \rightarrow C \rightarrow A$) makes it possible to account for all three phases if we assume that the $A \rightarrow B$ transition is fast (corresponding to phase 2), the $B \rightarrow C$ transition is of intermediate speed (corresponding to phase 3), and the $C \rightarrow A$ transition is slow; in such a scenario, states **A** and **C** can support or generate force (high force states) but state **B** cannot (detached, or low-force state). This model involves at least one ratchet mechanism. In this model, force can be generated by either of two transitions: $B \rightarrow A$ or $B \rightarrow C$. To determine which of these is the major force-generating step that consumes ATP and transduces energy, we examine the effects of ATP, ADP, and phosphate (Pi) on force transients. In doing so, we demonstrate that the fast transition (phase 2) is associated with the nucleotide-binding step, and that the intermediate-speed transition (phase 3) is associated with the Pi-release step. To account for all the effects of ligands, it is necessary to expand the three-state model into a six-state model that includes three ligand-bound states. The slowest phase of a force transient (phase 4) cannot be explained by any of the models described unless an additional mechanism is introduced. Here we suggest a role of series compliance to account for this phase, and propose a model that correlates the slowest step of the cross-bridge cycle (transition $C \rightarrow A$) to: phase 4 of step analysis, the rate constant k_{tr} of the quick-release and restretch experiment, and the rate constant k_{act} for force development time course following Ca^{2+} activation.

Keywords

Le Châtelier; Step analysis; Sinusoidal analysis; Tension; Kinetics; Rate constants; Two-state model; Three-state model; Phosphate; ATP; ADP

1 Introduction

Numerous contraction models involving multiple cross-bridge states have been proposed to account for isometric tension and tension transients, but many of them are not easy to follow

due to their mathematical complexity and the numerical approximations that are used for models. Indeed, the numerical approach makes it especially difficult to grasp the significance and usefulness of a particular model. Moreover, some models address only a part of the cycling scheme, and others rely on assumptions that are not clearly delineated. In an extreme case, too many cross-bridge states are employed and too many parameters are used to fit scanty data, which makes the reader wonder how much of the model is actually supported by the data on fiber studies, how much is an extrapolation from the data obtained from solution studies, and how much is pure speculation. Is a model with more cross-bridge states necessarily better than one with fewer? We believe that the purpose of the model is to account for experimental results, and to predict results for future experimentation. For this reason, we consider simplicity to be one of the key aspects of model building. In this mini-review, we focus on simple cases and attempt to explain some fundamental experimental observations. The mathematical principles used here are not complex and are, in fact, taught in high school and college courses. Hence if there are difficulties, one should consult with a math teacher or look into appropriate textbooks. Alternatively, the authors are always available for consultation. The cases covered here are limited to the isometric, or near-isometric, state of contraction; isotonic contraction is not dealt with because it introduces extra complexity. The mathematical symbols used in the text are summarized in Table 1.

2 The two-state model

This is the simplest model of all and, hence, easiest for beginners to understand while still of value for experts because it involves fundamental principles. The two-state model is extensively used in muscle physiology and in mechanics (e.g., Huxley 1957; Thorson and White 1969; Huxley and Simmons 1971; Abbot 1973; Brenner 1988; Palmer et al. 2007). When a reactant (**A**) changes into a product (**B**) with the forward rate constant α and its reversal rate constant α' , this kinetic scheme can be written as:

For application to muscle mechanics, state **A** is assigned to the attached “high force state”, and state **B** to the detached “no force state” (or low force state). The rate of the forward reaction is αA , and the rate of the reversal reaction is $\alpha' B$, where A and B represent the concentrations of the respective enzymatic species. Although concentration is usually written as $[A]$ and $[B]$, here the brackets are left out for simplicity and *italics* are used to denote mathematical variables. In contrast, when discussing molecular species we use bold letters such as **A** and **B**. As A and B are functions of time (t), they can be written as $A = A(t)$ and $B = B(t)$. In Scheme 1, because the forward rate is a loss and the reverse rate is a gain for **A**,

$$dA/dt = -\alpha A + \alpha' B \quad (1)$$

The reaction in Scheme 1 is called the first-order reaction because it is represented by the first-order differential equation (Eq. 1). Given that **A** and **B** are two forms of the same molecular species,

$$A + B = A_T \quad (2)$$

where A_T is the total concentration and is conserved (i.e., it does not change with time). In the case of concentrated solutions, the word “activity” is used in place of the concentration because not all molecules are chemically active. The consequent elimination of B from Eqs. 1 and 2 results in:

$$dA/dt + \lambda A = \alpha' A_T \quad (3)$$

$$\text{where } \lambda \equiv \alpha + \alpha' \quad (4)$$

Note that \equiv indicates definition. Equation 3 takes the form of Eq. A1 in Appendix 1, and it can be solved (Eq. A6) to result in:

$$A(t) = A_0 \exp(-\lambda t) + A_1 \quad (5)$$

$$\text{and } B(t) = -A_0 \exp(-\lambda t) + B_1 \quad (6)$$

$$\text{where } A_1 \equiv (\alpha' / \lambda) A_T \quad \text{and} \quad B_1 \equiv (\alpha / \lambda) A_T \quad (7)$$

Thus, the first-order reaction of Scheme 1 results in a time course with one exponential process whose rate constant is λ , which is the sum of the forward rate constant α and the reverse rate constant α' (Eq. 4). λ is termed the “apparent” rate constant, indicating that this is the rate constant experimentally observed as in Eq. 5 or 6. In contrast α and α' are termed the “intrinsic” or “fundamental” rate constants (Gutfreund 1995). Although the adjective “intrinsic”, “fundamental” or “apparent” is often left out, which of these would apply is usually self evident. A_0 is an integration constant that is determined by the initial condition, and it is termed the amplitude (or magnitude) of the exponential process in Eqs. 5 and 6.

As time approaches infinity ($t \rightarrow \infty$), Scheme 1 achieves an equilibrium, resulting in $dA(t)/dt = 0$ (in Eqs. 1 and 3). From Eqs. 5 and 6, it becomes clear that $A(\infty) = A_1$ and $B(\infty) = B_1$. Thus, $K \equiv \alpha/\alpha' = B_1/A_1$ is the equilibrium constant, and A_1 and B_1 are the equilibrium concentrations of individual molecular species. $K = B_1/A_1$ is the well-known law of mass action.

3 Perturbation

A perturbation (δx) is experimentally applied after the equilibrium described in Scheme 1 ($A = A_1$, $B = B_1$) is reached. The perturbation can be a length change (e.g., Thorson and White 1969; Huxley and Simmons 1971; Abbott 1973; Heinl et al. 1974; Kawai 1978), a temperature change (e.g., Bershitzky and Tsaturyan 1992; Davis and Rodgers 1995; Ranatunga 1999), a pressure change (e.g., Fortune et al. 1991), etc., but it must be small and fast. A perturbation can also be a sudden change in the ligand (ATP, ADP, Pi) concentration, such as that used in caged Pi (e.g., Homsher and Millar 1990; Dantzig et al. 1992; Walker et al. 1992; Araujo and Walker 1996), caged ATP (e.g., Goldman et al. 1984; Martin and Barsotti 1994), caged Ca (e.g., Preston et al. 2007), or rapid solution-switch (e.g., Tesi et al. 2000, 2002; Stehle et al. 2002; Piroddi et al. 2003) experiments. The purpose of the perturbation is to probe the rate constant(s) and to construct a kinetic scheme. In Scheme 1, the perturbation is assumed to modify the rate constants α and α' :

$$\alpha \rightarrow \alpha + \delta\alpha \quad (8)$$

$$\alpha' \rightarrow \alpha' + \delta\alpha' \quad (9)$$

$$\text{Therefore, } \lambda \rightarrow \lambda + \delta\lambda, \quad \text{where } \delta\lambda = \delta\alpha + \delta\alpha' \quad (10)$$

The changes described in Eqs. 8–10 are assumed to occur simultaneous to perturbation δx , with $\delta\alpha$ being the sensitivity of α , $\delta\alpha'$ the sensitivity of α' , and $\delta\lambda$ the sensitivity of λ , to perturbation δx . Because δx is a small quantity, all other δs are also small quantities.

The perturbation (Eqs. 8–10) results in a change in A that is time dependent:

$$A_1 \rightarrow A_1 + \delta A(t) \quad (11)$$

With the substitution of Eqs. 9, 10 and 11 into Eq. 3 we obtain:

$$d(A_1 + \delta A)/dt + (\lambda + \delta\lambda)(A_1 + \delta A) = A_T(\alpha' + \delta\alpha') \quad (12)$$

Sidewise subtraction of Eq. 3 from Eq. 12 gives:

$$d\delta A/dt + \lambda\delta A \cong A_T\delta\alpha' - A_1\delta\lambda \quad (13)$$

The cross term $\delta\lambda\delta A$ is dropped from Eq. 13 because this is an extremely small quantity. If preferred, Eq. 13 can be derived directly from Eq. 3 by differentiation. The right-hand side of Eq. 13 is a constant of time, because all variables are time-independent quantities. Note the similarity between Eqs. 3 and 13. By solving Eq. 13 (Appendix 1),

$$\delta A(t) = A_2[1 - \exp(-\lambda t)] \quad (14)$$

$$\delta B(t) = -\delta A(t) = -A_2[1 - \exp(-\lambda t)] \quad (15)$$

where $A_2 \equiv (A_T\delta\alpha' - A_1\delta\lambda)/\lambda = A_T(a\delta\alpha' - \alpha'\delta\alpha)/\lambda^2$. Note that we assume $\delta A(0) = 0$ (δA does not change immediately after the perturbation). A_2 is the amplitude (magnitude) of the exponential process, and the apparent rate constant in Eqs. 14 and 15 are the same as in Eq. 5. When a perturbation is applied to a muscle fiber, the resulting force time course, such as that described in Eqs. 14 or 15, is called “force transient” or “tension transient”.

Conclusion 1

An experimenter will observe the same rate constant λ whether starting a new reaction as in Scheme 1 (Eq. 5), or applying a small perturbation (of any kind) during equilibrium and measuring the transient as in Eq. 14. Although not shown explicitly, this conclusion holds true for any multiple-state model.

4 Tension transients and delayed tension

When an isometrically contracting muscle fiber is stretched by δl (with $\delta l < 0$ in the case of release), force rises simultaneous to the stretch because of the elastic link of attached cross-bridges. This is termed phase 1 (Fig. 1A; Huxley and Simmons 1971; Heintz et al. 1974). Force then decays quickly (phase 2), after which it again rises, but more gradually (phase 3 in Fig. 2). Phase 3 is particularly evident in insect indirect flight muscles (Fig. 3A; Pringle 1978), and is called “delayed tension”. To explain the delayed tension, Thorson and White (1969, 1983) used the two-state model, but had to assume that either α' increases (as does in Huxley's model 1957, and in Julian et al.'s model 1974) or α decreases with a stretch (δl), in other words, that $\delta\alpha'/\delta l > 0$ or $\delta\alpha/\delta l < 0$ (see also Abbott 1973; Abbott and Steiger 1977; Pringle 1978). The perturbation analysis used was exactly the same as in Eqs. 8–14 above. This assumption ($\delta\alpha'/\delta l > 0$ or $\delta\alpha/\delta l < 0$), however, does not satisfy the Le Châtelier–Brown Principle, which states that a thermodynamic system tends to balance the effects of any stress inflicted upon it (Kirkwood and Oppenheim 1961). In the case of muscle mechanics, this principle is interpreted in the following way.

If a cross-bridge that is generating force (φ) is stretched by δl , then the work (δW) performed by the forcing apparatus on this cross-bridge is:

$$\delta W = (\text{force}) \times (\text{distance}) = \varphi \delta l \quad (16)$$

Equation 16 also holds true for release ($\delta l < 0$), in which case $\delta W < 0$ and the work is performed by the cross-bridge on the forcing apparatus. φ is force/cross-bridge ($\varphi > 0$), and the same as the unitary force used in single molecule experiments (e.g. Molloy et al. 1995; Guilford et al. 1997; Kitamura et al. 1999). It is likely that the unitary force is distributed because the mismatch between actin and myosin repeats in most muscles causes the strain on cross-bridges to be distributed. Thus, it is more accurate to state that φ represents the averaged unitary force over the distributed strain. From here, there are two possibilities: in case 1, the activation energy E_α for the reaction $\mathbf{A} \rightarrow \mathbf{B}$ is reduced by the stretch (Fig. 4A); in case 2, the activation energy E'_α for the reversal reaction $\mathbf{B} \rightarrow \mathbf{A}$ is increased by the stretch (Fig. 4B). In case 1, the chain of events is $\delta l \rightarrow \delta W \rightarrow \delta E_\alpha \rightarrow \alpha$, which results in a change in the rate αA .

$$\delta E_\alpha = -\delta W = -\varphi \delta l \quad (17)$$

The rate constant α is related to the activation energy by the Arrhenius equation (Gutfreund 1995):

$$\alpha = \alpha_0 \exp(-E_\alpha/k_B T) \quad (18)$$

where k_B is the Boltzmann's constant, and T is the absolute temperature. By differentiation of Eq. 18 with respect to E_α , we obtain

$$\delta\alpha = -\frac{\alpha_0}{k_B T} \exp\left(-\frac{E_\alpha}{k_B T}\right) \delta E_\alpha = -\frac{\alpha}{k_B T} \delta E_\alpha \quad (19)$$

From Eqs. 17 and 19, we get

$$\frac{\delta\alpha}{\alpha} = \frac{\varphi}{k_B T} \delta l \quad (20)$$

For case 2, the chain of events is $\delta l \rightarrow \delta W \rightarrow \delta E'_\alpha \rightarrow \alpha'$ and this changes the reversal rate α' . Here, because $\delta E'_\alpha = +\delta W$, the expression equivalent to Eq. 20 is

$$\frac{\delta\alpha'}{\alpha'} = -\frac{\varphi}{k_B T} \delta l \quad (21)$$

From Eq. 20, $\delta\alpha/\delta l = \alpha\varphi/k_B T > 0$ (it cannot be negative). Similarly, from Eq. 21, $\delta\alpha'/\delta l = -\alpha'\varphi/k_B T < 0$ (it cannot be positive). That is, in response to stretch ($\delta l > 0$), E_α decreases ($\delta E_\alpha < 0$, Eq. 17) and α increases (Eq. 20) (case 1), or E'_α increases ($\delta E'_\alpha > 0$) and α' decreases (Eq. 21) (case 2). Consequently, A should gradually decrease (phase 2) in both cases, as in the Huxley and Simmons (1971) model, rather than gradually increasing (phase 3). As is clear from the above discussion, the two-state model can explain phase 2, but not phase 3 (the well-known phenomenon of “delayed tension”). Actually, this problem can be circumvented by postulating that the stretch increases the number of cross-bridges in the **B** state (no tension state) instantly, making it possible to explain the delayed rise in tension as **B** \rightarrow **A** in Scheme 1 occurs; i.e. the tension rises with the rate constant λ (Eq. 5), as considered in Section 9. In terms of case 1 vs. case 2 discussed above, certain lines of experimental evidence favor case 2, based on the asymmetry of the apparent rate constant ($\lambda = \alpha + \alpha'$) of phase 2, which decreases with stretch (Huxley and Simmons 1971; Ford et al. 1977).

5 The expanded two-state model

When attached cross-bridges **A** are stretched by δl , they follow different kinetics from ones that are not stretched. One way of simplifying this complication is to consider that the stretched cross-bridges are in a special state **G**, as shown in Scheme 2. As time progresses, **G** decays at the rate constant μ to become **B**, and is not regenerated. This aspect is in contrast to the two-state model discussed in Section 4, in which the stretched state can be regenerated. In Scheme 2, state **A** vanishes at the time of stretch, but because the **B** \leftrightarrow **A** transition takes place, **A** reappears over time.

The following differential equations (Eqs. 22–24) describe the kinetics of Scheme 2:

$$dA(t)/dt = -\alpha A + \alpha' B \quad (22)$$

$$dB(t)/dt = \alpha A - \alpha' B + \mu G \quad (23)$$

$$dG(t)/dt = -\mu G \quad (24)$$

$$\text{Evidently } A(t)+B(t)+G(t)=A_1 \quad (25)$$

The initial conditions and the final steady state concentrations are:

$$\begin{aligned} A(-0) &= A_1, & A(+0) &= 0, & A(\infty) &\equiv A_1 \\ B(-0) &= B_1, & B(+0) &= B_1, & B(\infty) &\equiv B_1 \\ G(-0) &= 0, & G(+0) &= A_1, & G(\infty) &\equiv G_1 = 0 \end{aligned}$$

where $t = -0$ means immediately before the stretch, and $t = +0$ means immediately after the stretch. A_1 and B_1 are defined in Eq. 7. Eqs. 22–25 can be solved in reverse order, i.e. first yielding $G(t)$ (Appendix 1), then $B(t)$, and finally $A(t)$. Alternatively, the method described in Appendix 2 for three states can be used, because the expanded two-state model is a special case of the three-state model. The results are as follows.

$$A(t) = A_1 + \frac{A_1}{\alpha' - \delta\alpha} [\delta\alpha \exp(-\lambda t) - \alpha' \exp(-\mu t)] \quad (26)$$

$$B(t) = B_1 + \frac{\delta\alpha}{\alpha' - \delta\alpha} A_1 [-\exp(-\lambda t) + \exp(-\mu t)] \quad (27)$$

$$G(t) = A_1 \exp(-\mu t) \quad (28)$$

$$\text{where } \mu \equiv \alpha + \delta\alpha$$

λ is defined in Eq. 4. $\lambda > \mu$, because $\alpha' > \delta\alpha$ when δ is small. Relating a chemical state to force can be simplified by considering a myofibril of cross sectional area A_C and a half sarcomere of length l_0 . Because all cross-bridges in this structure are arranged in parallel mechanically, the forces generated (or supported) by state **A** (F_A) and state **B** (F_B) are proportional to the number of force generating cross-bridges in each state.

$$\begin{aligned} F_A &= \varphi A A_C l_0 N_A \\ F_G &= (\varphi + \rho \delta l) G A_C l_0 N_A \end{aligned}$$

φ is the force/cross-bridge (unitary force) in state **A**, $\varphi + \rho \delta l$ is the force/cross-bridge in state **G**, ρ is the spring constant of the cross-bridge, and N_A is Avogadro's number. Therefore, in the half sarcomere $A A_C l_0 N_A$ is the total number of cross-bridges in state **A**, and $G A_C l_0 N_A$ is the total number of cross-bridges in state **G**. Force $F(t)$ is:

$$\begin{aligned} F(t) &= F_G + F_A = [\varphi(A+G) + G\rho\delta l] A_C l_0 N_A \\ &= A_1 [\varphi - z \exp(-\mu t) + w \exp(-\lambda t)] A_C l_0 N_A \end{aligned} \quad (29)$$

$$\text{where } z \equiv \varphi\delta\alpha/(\alpha' - \delta\alpha) - \rho\delta l \quad (30)$$

$$\text{and } w \equiv \varphi\delta\alpha/(\alpha' - \delta\alpha) \quad (31)$$

$$\begin{aligned} F(-0) &= \varphi A_1 A_c l_0 N_A \\ F(+0) &= A_1 (\rho\delta l + \varphi) A_c l_0 N_A \\ F(\infty) &= \varphi A_1 A_c l_0 N_A \end{aligned}$$

Equations 29, 30, and 31 illustrate that a force transient comprises three phases. The first is a rise in the force simultaneous with the stretch. The second is a rapid decay of force at rate constant μ , and reflects the decay of \mathbf{G} . The outcome of the third phase depends on the polarity of z : if $z > 0$, then there is a delayed rise in force as it approaches $A_1 A_c l_0 N_A$; if $z \leq 0$, then there is further decay of force to the steady state value $A_1 A_c l_0 N_A$. Although this model (Scheme 2) may appear to explain the delayed tension when $z > 0$, in fact it does not quite accomplish this because the rise of force is small and never exceeds the steady-state value.

According to the above analysis, the length change can be seen to induce an extra state \mathbf{G} , which decays with a unique rate constant (μ). Steiger and Abbott (1981) used this line of modeling on a four-state model (with two attached and two detached states after Lynn and Taylor 1971), to generate one with six states. Although we believe that Scheme 2 and its theory represent one of the most rigorous systems for treating the stretched (or released) cross-bridges, they may not allow for practical analysis of experimental results because the apparent rate constants λ and μ are similar and, hence, difficult to distinguish from one another. In addition, modeling must include one extra cross-bridge state per attached cross-bridge state, which adds to the complexity of the algebra required when multiple attached states are considered. For these reasons, we do not use this line of approach in the following discussions.

6 The three-state model

To explain delayed tension more explicitly, it is necessary to introduce the three-state model. Given the extreme usefulness of this model, we discuss it in detail. The three state model has been used frequently among muscle physiologists and mechanics (e.g., Julian et al. 1974; Thorson and White 1983; Woledge et al. 1985; Murase et al. 1986; Dickinson et al. 1997; Campbell et al. 2001). Scheme 3 represents its most general form.

This is a cyclic scheme with the forward reaction consisting of the outer clockwise cycle: $\mathbf{A} \rightarrow \mathbf{B} \rightarrow \mathbf{C} \rightarrow \mathbf{A}$, for which the respective rate constants are α, β and γ . The reversal reaction consists of the inner counter-clockwise cycle: $\mathbf{A} \rightarrow \mathbf{C} \rightarrow \mathbf{B} \rightarrow \mathbf{A}$, with the respective rate constants γ', β' and α' . In Scheme 3, we assume that \mathbf{A} and \mathbf{C} are attached states, which generate and/or support force, and that \mathbf{B} is a detached state, which does not support force. Because the analysis of Scheme 3 is very complex, we will discuss a simple case here. The complete analysis of Scheme 3 can be found in the Appendix 2.

7 Three-state model, a simple case analysis ($\alpha + \alpha' \gg \beta + \beta' \gg \gamma + \gamma'$)

Now let us consider a simple case in which $\alpha + \alpha' \gg \beta + \beta' \gg \gamma + \gamma'$ is satisfied. In the following discussion, these rate constants are referred to fast, medium, and slow, respectively. The case

$\alpha + \alpha' \ll \beta + \beta' < \gamma + \gamma'$ is included in this discussion by an exchange: $\alpha, \alpha' \leftrightarrow \gamma, \gamma'$. The more realistic case ($\alpha + \alpha' > \beta + \beta' > \gamma + \gamma'$) is discussed later in Section 20. $X \gg Y$ indicates that X is much larger than Y , so that Y can be ignored when $X + Y$ is evaluated. An example is 1000 s^{-1} and 100 s^{-1} . If we focus on a fast time scale, comparable to $1/(\alpha + \alpha')$ (such as $\sim 1 \text{ ms}$ in the cross-bridge cycle), then steps 2 ($\mathbf{B} \leftrightarrow \mathbf{C}$) and 3 ($\mathbf{C} \leftrightarrow \mathbf{A}$) are too slow to occur. Hence they could not be witnessed on the time-scale of observation. In this case, only step 1 is observed, and the problem is reduced to Scheme 1, with the apparent rate constant λ_2 .

$$\lambda_2 = \alpha + \alpha' \quad (32)$$

Conclusion 2

The apparent rate constant of a fast step (λ_2) is the sum of the forward rate constant and the reversal rate constant of this step (Eq. 32), and it is not influenced by either the rate or equilibrium constants of slower steps.

If we focus on a medium-speed time scale, comparable to $1/(\beta + \beta')$ (such as $\sim 10 \text{ ms}$ in the cross-bridge cycle), then step 1 is very fast and looks like an equilibrium, whereas step 3 is too slow to be witnessed. Therefore, in this scenario, Scheme 3 actually looks like Scheme 4.

where $K_\alpha \equiv \alpha/\alpha'$, which is the equilibrium constant of step 1. In this case

$$\frac{d(A+B)}{dt} = -\beta B + \beta' C \quad (33)$$

That is, **A** and **B** gain/lose as a group. Because **A**, **B** and **C** are three different states of myosin,

$$A+B+C=A_T \quad (34)$$

where A_T is the total concentration of myosin subfragment one (S1). Because step 1 represents an equilibrium, the mass action law applies:

$$B/A = K_\alpha \quad (35)$$

By eliminating B and C from Eqs. 33–35, we obtain

$$dA/dt + \lambda_3 A = \beta' A_T / (1 + K_\alpha) \quad (36)$$

$$\text{where } \lambda_3 \equiv \frac{K_\alpha}{1 + K_\alpha} \beta + \beta' \quad (37)$$

By solving Eq. 36 (Appendix 1), we arrive at:

$$\begin{aligned} A(t) &= A_0 \exp(-\lambda_3 t) + A_1, & B(t) &= A_0 K_\alpha \exp(-\lambda_3 t) + B_1, \\ C(t) &= -A_0(1 + K_\alpha) \exp(-\lambda_3 t) + C_1 \end{aligned} \quad (38)$$

where $A_1 \equiv A_T/[1 + K_\alpha(1 + K_\beta)]$, $B_1 = K_\alpha A_1$ and $C_1 = K_\alpha K_\beta A_1$ are the steady-state concentrations, and $K_\beta \equiv \beta/\beta'$ is the equilibrium constant of step 2. Equation 38 shows that Scheme 4 has the apparent rate constant λ_3 , which is defined in Eq. 37.

Conclusion 3

The apparent rate constant of a medium-speed step (λ_3) is a weighted sum of the intrinsic rate constants β and β' of step 2; although λ_3 is influenced by the equilibrium constant of the fast steps, it is not influenced by the rate or equilibrium constants of the slow steps.

Thus, the three-state model (Scheme 3) has 2 exponential processes with 2 apparent rate constants, λ_2 and λ_3 ($\lambda_2 > \lambda_3$) (generally, an N-state model has (N-1) exponential processes). Each apparent rate constant is the weighted sum (linear combination) of the forward and reversal rate constants of the respective steps (Eqs. 32 and 37). The time courses $A(t)$, $B(t)$ and $C(t)$ take the form described in Eqs. A21–A23 of Appendix 2. Step 3 occurs slowly, which is important for calculation of the turnover rate. In perturbation analysis, the rate constants of the fast steps (1 and 2) can be observed (Eqs. 32 and Eq. 37), whereas the rate constant of the slowest step (3) cannot be observed. However, because of the presence of in-series compliance, the forward rate constant of step 3 can be observed as discussed later in Section 19.

8 Steady state

In Scheme 3, $t \rightarrow \infty$ will result in the steady state, in which $dA(t)/dt = 0$, $dB(t)/dt = 0$, and $dC(t)/dt = 0$ are achieved. From these conditions, it follows that the steady-state concentrations of A_1 , B_1 , C_1 (still assuming that $\gamma, \gamma' \ll \alpha, \alpha', \beta, \beta'$) are:

$$A_1 = A_T \alpha' \beta' / M, \quad B_1 = A_T \alpha \beta' / M, \quad C_1 = A_T \alpha \beta / M \quad (39)$$

$$\text{where } M \equiv \alpha\beta + \alpha\beta' + \alpha'\beta'$$

The turnover rate J is calculated as:

$$J = \gamma C_1 - \gamma' A_1 = A_T (\alpha\beta\gamma - \alpha'\beta'\gamma') / M \quad (40)$$

In the case of the cross-bridge cycle, J is the same as the ATP hydrolysis rate. The equilibrium is a special case ($J = 0$) of the steady state. If $\alpha A_1 - \alpha' B_1$ or $\beta B_1 - \beta' C_1$ is evaluated in place of Eq. 40, both become 0 because of the approximations we used. In this case, $B_1/A_1 = \alpha/\alpha' = K_\alpha$, and $C_1/B_1 = \beta/\beta' = K_\beta$. Hence, step 1 and step 2 can be approximated by the equilibrium. However, although $C_1/A_1 = \alpha\beta/\alpha'\beta' = K_\alpha K_\beta$, generally $A_1/C_1 \neq \gamma/\gamma'$. Hence, step 3 does not contribute to the equilibrium of the reaction $C \leftrightarrow A$ (step 3) directly, but rather steps 1 and 2 (reactions $A \leftrightarrow B \leftrightarrow C$) determine the equilibrium.

Conclusion 4

At steady state, the fast steps of the cyclic reaction can be approximated by the equilibrium, whereas the slowest (rate-limiting) step cannot be approximated by the equilibrium.

9 The mechanisms of tension transients that satisfy the Le Châtelier–Brown Principle

Based on Scheme 3, it is now possible to explain delayed tension without violating the Le Châtelier–Brown Principle. When the length of active muscle fiber is stretched ($\delta l > 0$) rapidly, force increases simultaneously because of the combined effect of attached cross-bridge elasticity and series compliance (phase 1, Figs. 1A and 2). The stretch simultaneously increases the elastic energy δW (mechanical energy) stored in the cross-bridge state **A** (Eq. 16); hence it either reduces the activation energy E_α (Eq. 17; Fig. 4A) or elevates the activation energy E'_α (Fig. 4B). This increases the rate constant α (Eq. 20) and/or decreases the rate constant α' (Eq. 21), and thus increases the **A** \rightarrow **B** transition and/or decreases the **B** \rightarrow **A** transition to reduce the energy and to satisfy the Le Châtelier–Brown Principle. In either case, the result is an exponential decay of force (phase 2, Fig. 1A) at rate constant λ_2 (Eq. 32), and is consistent with the model proposed by Huxley and Simmons (1971). Step 2 (**B** \rightarrow **C**) is slower and does not take place at this time. Over time, cross-bridges accumulate in the **B** state. The amount of this accumulation is substantial, as the following calculations demonstrate. From Eq. 7,

$$\frac{1}{B_1} \left(\frac{\partial B_1}{\partial \alpha} \right)_{\alpha'} = \frac{\alpha'}{\alpha \lambda} \quad (41)$$

$$\text{and} \quad \frac{1}{B_1} \left(\frac{\partial B_1}{\partial \alpha'} \right)_{\alpha} = -\frac{1}{\lambda} \quad (42)$$

In case 1 (Section 4), a side-wise multiplication of Eq. 20 to Eq. 41 yields Eq. 43.

$$\begin{aligned} \frac{\delta B_1}{B_1} &= \frac{\alpha'}{\lambda kT} \delta l \\ &= \frac{1 \times 2 \text{ pN}}{2 \times 1.38 \times 10^{-23} \text{ JK}^{-1} \times 293 \text{ K}} \times 0.75 \text{ nm} = 0.19 \end{aligned} \quad (43)$$

In case 2 (Section 4), a side-wise multiplication of Eq. 21 by Eq. 42 likewise yields Eq. 43. Here we assumed that unitary force (φ) is 2 pN (range 1–6 pN: Finer et al. 1994; Miyata et al. 1995; Molloy et al. 1995; Ishijima et al. 1996; Guilford et al. 1997), the value of α is comparable to that of α' , $T = 293 \text{ K}$ (20°C), and the length change is 0.1% stretch. Consequently, $\delta l = 0.001 \times 1.25 \mu\text{m} \times 60\% = 0.75 \text{ nm}$, where half sarcomere length is $1.25 \mu\text{m}$, at which skinned psoas fiber experiments are usually carried out. 60% is to account for cross-bridge compliance, and the remaining 40% series compliance; the results with respect to the temperature effect on stiffness (rabbit psoas fibers) fit well if the series compliance is $40 \pm 5\%$ during standard activation at 20°C (Kawai 2003). The reported series compliance varies significantly, the lowest value being 19% (Bagni et al. 1990) and the highest 69% (Wakabayashi et al. 1994), and mid-range values having been published as well (44% in Higuchi et al. 1995 and 50–60% in Dobbie et al. 1998). Equation 43 suggests that the number of cross-bridges in state **B** increases as much as 19% in response to a stretch as small as 0.1%. The increase becomes

about 38% for a 0.2% stretch, and so on. Here it is possible that a “ratchet” mechanism is at work in step 1 (i.e., preferred detachment of unstrained, or perhaps negatively strained, cross-bridges: Huxley 1957; Vale and Oosawa 1990; Smith and Geeves 1995; Smith 1998), increasing the number of cross-bridges in state **B** even further. However, it must be recognized that the ratchet mechanism is against the Le Châtelier-Brown principle, thereby the ratchet has its value.

The next thing that happens is an increase in the slower step 2 (**B** → **C**), because its rate is βB , and the number (B) of cross-bridges in state **B** is now larger than steady-state ($\delta B_1 > 0$: Eq. 43). The stretch also increases the elastic energy in state **C**, which in turn reduces the activation energy E'_β . Hence β' is also accelerated (or E_β is elevated and β is diminished). Consequently, the reversal reaction of step 2 (**C** → **B**) is accelerated. The net reaction is the sum of those in both directions, with the rate constant λ_3 (Eq. 37). When the rate βB (**B** → **C**) is greater than the rate $\beta' C$ (**C** → **B**), we observe a delayed rise in tension (phase 3, Figs. 2 and 3A); when the rates are equal, we observe a plateau (phase 3, Fig. 1A); when βB is less than $\beta' C$, we do not observe the delayed rise in tension. The above-mentioned ratchet mechanism is important here, because the projected rate $\beta' C$ is large and comparable to βB . In addition, there may be a ratchet mechanism in step 2 to decelerate the reversal reaction **C** → **B**. Because the amplitude (magnitude B in sinusoidal analysis) of phase 3 is smaller in frog semitendinosus fibers than that in rabbit psoas fibers under the same activating condition (Kawai and Brandt 1980), phase 3 in frog fibers shows a plateau in step analysis (Fig. 1A). The amplitude is sizable in rabbit psoas fibers. Hence a delayed rise in tension is clearly visible (Fig. 2). We have also noticed that the presence of exponential process B (phase 3) depends on the goodness of the fiber preparation; if it is poor, phase 3 magnitude is less, or it even disappears.

A mirror image of the above events occurs on release ($\delta l < 0$) of the active muscle fibers. On release, force drops (phase 1, Figs. 1B and 3B) due to simultaneous release of the combined elasticity of series compliance and the attached cross-bridges. This results in a decrease in the elastic energy stored in state **A** (Eq. 16), which in turn increases E_α (Eq. 17) and reduces α (Eq. 20) (or reduces E'_α and increases α') to satisfy the Le Châtelier–Brown Principle. Thus, the rate αA decreases (or $\alpha' B$ increases). Because there is a continuous supply of **A** via **B** → **A** and **C** → **A** transitions, the net effect is a transient increase (accumulation) of state **A**, and a transient decrease of state **B**. Overall, this results in an exponential rise of force (phase 2, Fig. 1B), at a rate constant λ_2 (Eq. 32). Step 2 is slower and does not take place yet. The result over time is a temporary decrease in the cross-bridges of the **B** state and, as seen from Eq. 43, this decrease is substantial. The next event is the slower step 2. The rate of its forward reaction βB (**B** → **C**) is now reduced because B is reduced. The elastic energy stored in state **C** decreases with the release of length; hence the activation energy is increased and the rate constant β' reduced, resulting overall in a decline of the rate of the reversal reaction $\beta' C$ (**C** → **B**). Again, the net reaction is the sum of those in both directions, with rate constant λ_3 . When rate $\beta' C$ (**C** → **B**) is greater than rate βB (**B** → **C**), we observe a delayed drop in tension (phase 3, Fig. 3B); when the rates are equal, we observe a plateau (phase 3, Fig. 1B); and when rate $\beta' C$ (**C** → **B**) is weaker than rate βB (**B** → **C**), we do not observe a delayed drop in tension. Recently, Burton et al. (2006) presented a case in which the polarity of phase 3 and 4 was in the same direction when a large (1%) release in rabbit psoas fiber was tested. Thus, polarity of phase 3 may be determined by the experimental conditions.

In all cases, the transitions satisfy the Le Châtelier–Brown Principle. From the above discussion, it is clear that phase 2 represents **A** ↔ **B** interconversion (step 1), with the fast apparent rate constant of λ_2 , and that phase 3 represents **B** ↔ **C** interconversion (step 2), with the medium apparent rate constant λ_3 as indicated in Scheme 3. What it is important to notice here is that both phase 2 of stretch and phase 2 of release arise from the same elementary step of the cross-bridge cycle, because tension transients on stretch and release are almost in mirror

image to each other (Figs. 1 and 3). Similarly, phase 3 of stretch and phase 3 of release arise from the same elementary step. Due to energetic considerations (Eqs. 16–21), however, the resulting rate constants for stretch and release are asymmetric. This is referred to as “non-linearity” of the rate constants (Huxley and Simmons 1971), and accounts for the fact that tension transients are not in perfect mirror image on stretch and release, as shown in Fig. 1A and 1B. From the above discussions, it can be concluded that tension develops (increases) by two mechanisms: through the fast $\mathbf{B} \rightarrow \mathbf{A}$ transition (phase 2) that occurs on release (counter-clockwise cycle in Scheme 3; Fig. 1B), and through the medium-speed $\mathbf{B} \rightarrow \mathbf{C}$ transition (phase 3) that occurs on stretch (clockwise cycle; Figs. 2 and 3A).

Conclusion 5

The three-state model (Scheme 3) can explain phase 2 and phase 3 of force transients without violating the Le Châtelier–Brown Principle, provided that step 3 is the rate-limiting step, the middle state (\mathbf{B}) is a low-or no-force state, and there is a ratchet mechanism to increase the $\mathbf{A} \rightarrow \mathbf{B}$ transition or to diminish the $\mathbf{C} \rightarrow \mathbf{B}$ transition in response to stretch. Both states \mathbf{A} and \mathbf{C} must bear force, and step 1 must be faster than step 2.

In performing perturbation experiments in muscle fibers and probing the elementary steps of the cross-bridge cycle, it is important to keep the length change small. We typically use a sinusoidal length change with a 0.25% peak-to-peak amplitude, which corresponds to 1.9 nm (or ± 0.95 nm) at the cross-bridge level when 40% series compliance is considered. Because this is smaller than the step size (4–11 nm: Molloy et al. 1995; Guilford et al. 1997; Kitamura et al. 1999), the elementary steps can be probed. A 10% length change, by contrast, corresponds to 75 nm at the cross-bridge level, and the cross-bridge would have to cycle many (7 to 19) times to compensate for this large length change. The time course of such an experiment would be limited by the slowest step of the cycle. As is seen in Eq. 43, even a small length change has a strong effect on cross-bridge occupancy, and therefore results in a large change in force.

10 Effects of MgATP and phosphate (Pi)

The next question is whether, in Scheme 3, cross-bridges cycle in the clockwise direction or in the counter-clockwise direction to consume ATP and to perform work. To answer this, we need to look into the effects the substrate (MgATP) and product (phosphate and MgADP) concentrations have on the apparent rate constants.

In rabbit psoas fibers, an increase in the the MgATP concentration was shown to accelerate the rate constants of phases 2 and 3 in sinusoidal length-change experiments (Kawai 1978). In sinusoidal analysis, the apparent rate constant of phase 2 is termed $2\pi c$, and that of phase 3 is termed $2\pi b$ (see Scheme 3). Because the temporal resolving power (signal-to-noise ratio) is greater in sinusoidal length-change experiments than in step length-change experiments, we adapted this technique. According to conclusions 2 and 3 above, the effect of ATP implies that the MgATP binding is associated with a fast reaction step whose rate constant is comparable to $2\pi c$. We have also found that an increase in the Pi concentration accelerates the rate constant of phase 3 ($2\pi b$), but that Pi does not significantly affect the rate constant of phase 2 ($2\pi c$) (Kawai 1986). In light of conclusion 3, this observation implies that the Pi binding step is coupled to a medium-speed step with a rate constant comparable to $2\pi b$. If we fit these results to Scheme 3, then it follows that ATP binding is associated with step 1, whereas Pi binding is associated with step 2. These possibilities are considered quantitatively in the following Sections 11–13.

11 Substrate-binding step with a conformational change

To indicate a cross-bridge state we now use \mathbf{X}_i ($i = 0, 1, 2, \dots$). When X_i is used in algebraic expressions, we define it as the probability of the cross-bridge state, rather than the concentration. Because substrate (**S**) binding to cross-bridges at \mathbf{X}_1 is rapid, this reaction can be described by an equilibrium with association constant K_1 . The basis for this is that the binding reaction starts with a diffusion-limited collision between **S** and \mathbf{X}_1 , and the resulting product, \mathbf{X}_2 , is the state immediately after the collision (collision complex). \mathbf{X}_2 then undergoes a slower conformational change (isomerization) to become \mathbf{X}_3 :

The math that corresponds to Scheme 5 is identical to that of Scheme 4 with the following substitutions: \mathbf{X}_1 in place of **A**, \mathbf{X}_2 in place of **B**, \mathbf{X}_3 in place of **C**, K_1S in place K_a , k_2 in place of β , and k_{-2} in place of β' (note, however, that we are not correlating **A** to \mathbf{X}_1 , **B** to \mathbf{X}_2 , etc). In this substitution, S is the substrate (MgATP) concentration and a constant over time in skinned fiber experiments, because the muscle preparation is bathed in a large volume of solution with a fixed MgATP concentration; the solution is usually buffered by the ATP regenerating system, creatine phosphate and creatine kinase (CP/CK) or the equivalent (see, however, Cooke and Pate (1985) for a problem with this approach). Therefore, equations to describe Scheme 5 can be derived from Eqs. 33–36, with the above substitutions, and the results can be calculated using Eq. 37. That is, Scheme 5 has the apparent rate constant:

$$\lambda_2 = \frac{K_1 S}{1 + K_1 S} k_2 + k_{-2} \quad (44)$$

Thus, λ_2 increases and saturates hyperbolically with an increase in S . The data of $2\pi c$ vs. S that were obtained from rabbit psoas fibers were fitted to Eq. 44 to derive three kinetic constants ($K_1 = 1.4 \text{ mM}^{-1}$, $k_2 = 440 \text{ s}^{-1}$, $k_{-2} = 100 \text{ s}^{-1}$ at 20°C : Kawai and Halvorson 1989) that characterize Scheme 5. Based on caged ATP experiments, Goldman et al. (1984) reported that the second order rate constant of cross-bridge detachment is at least $500 \text{ mM}^{-1} \text{ s}^{-1}$ (rabbit psoas, $20\text{--}22^\circ\text{C}$). This number is equivalent to $K_1 k_2$ (initial slope of Eq. 44) of Scheme 5, and is in approximate agreement with the value calculated from it ($1.4 \text{ mM}^{-1} \times 440 \text{ s}^{-1} = 620 \text{ mM}^{-1} \text{ s}^{-1}$). The NPE-caged ATP that was used did not allow faster rate constants to be probed, in part because of the slow rate of photolysis ($\sim 100 \text{ s}^{-1}$) (Goldman et al. 1984) and also because of its competition with ATP (Thirlwell et al. 1995). Hence, the saturation phase of Eq. 44 cannot be defined based on caged ATP experiments. Sinusoidal analysis does not have these limitations. Hence Eq. 44 has been utilized extensively to characterize other fasttwitch (Galler et al. 2005) and slow-twitch (Wang and Kawai 1996) skeletal muscle fibers, and porcine (Zhao and Kawai 1996) and bovine (Fujita et al. 2002) myocardium as well as *Drosophila melanogaster* indirect flight muscles (Swank et al. 2006), as summarized in Table 2. Solution studies of S1 from rabbit back muscles (performed at $20\text{--}23^\circ\text{C}$) yielded $K_1 = 4.5 \text{ mM}^{-1}$, $k_2 = 400 \text{ s}^{-1}$, and $k_{-2} < 0.02 \text{ s}^{-1}$ (Bagshaw et al. 1974), and similar studies of actoS1 (performed at 20°C) yielded $K_1 k_2 = 1500 \text{ mM}^{-1} \text{ s}^{-1}$ (Millar and Geeves 1988). Similarly, studies of myofibril suspension (at 20°C) yielded $K_1 k_2 = 1800 \text{ mM}^{-1} \text{ s}^{-1}$ and $k_{-2} \sim 0$ (Herrmann et al. 1994). Thus, it can be concluded that K_1 and k_2 were in approximate agreement in four very different preparations.

From the above discussion, it is clear that \mathbf{X}_1 and \mathbf{X}_2 correspond to state **A** in Scheme 3, and that \mathbf{X}_3 corresponds to state **B**. This assignment cannot be transposed because that would require that the slow rate constant, $\lambda_3 (= 2\pi b)$, decreases as S increases, yet $2\pi b$ was found to increase concomitant with an increase in the MgATP concentration (Kawai 1978; Kawai and Zhao 1993). This assignment demonstrates that a cross-bridge cycles in the clockwise direction in Scheme 3. With regard to the ratchet mechanism discussed in Section 9, we have

experimental evidence that K_1 (ATP binding) becomes larger as isometric tension is decreased by various experimental manipulations (Zhao et al. 1996), indicating that cross-bridges detach more readily as load is reduced. This mechanism is consistent with the Fenn effect (Fenn 1923).

12 ADP as a competitive inhibitor of ATP

It has been shown that an increase in the MgADP concentration results in a decrease in the rate constants of phase 2 and phase 3 (Kawai 1986; Kawai and Halvorson 1989). This result can be interpreted as the effect of a competitive inhibitor (Scheme 6).

where \mathbf{D} is MgADP, K_0 is the association constant for \mathbf{D} to \mathbf{X}_1 , and \mathbf{X}_0 is the ADP-bound state. It is known that myosin S1 has only one nucleotide-binding site (Rayment et al. 1993), and that it can bind either MgATP or MgADP. In Scheme 6, K_0 is written underneath the reaction, because the association is the reversal reaction, from \mathbf{X}_1 to \mathbf{X}_0 .

Because \mathbf{X}_0 , \mathbf{X}_1 and \mathbf{X}_2 lose and gain as a group in Scheme 6, Eq. 45 can be set up.

$$d(X_0+X_1+X_2)/dt = -k_2X_2 + k_{-2}X_3 \quad (45)$$

From the mass action law,

$$K_0 = X_0/X_1D \quad \text{and} \quad K_1 = X_2/X_1S \quad (46)$$

where D is the MgADP concentration. Because X_i is the probability,

$$X_0 + X_1 + X_2 + X_3 = X_T \quad (47)$$

where X_T is a constant of time while we make the observation at the high speed. By eliminating X_0 , X_1 and X_2 from Eqs. 45–47, we arrive at:

$$dX_3/dt + \lambda_2 X_3 = \varepsilon k_2 \quad (48)$$

$$\text{where} \quad \varepsilon \equiv K_1 S / (1 + K_0 D + K_1 S) \quad (49)$$

$$\text{and} \quad \lambda_2 \equiv \varepsilon k_2 + k_{-2} = \frac{K_1 S}{1 + K_0 D + K_1 S} k_2 + k_{-2} \quad (50)$$

From Eq. 48 (Appendix 1), we get:

$$\begin{aligned} X_3(t) &= X_{30} \exp(-\lambda_2 t) + X_{31}, \\ X_2(t) &= -\varepsilon X_{30} \exp(-\lambda_2 t) + X_{21}, \quad \text{etc.} \end{aligned} \quad (51)$$

where X_{30} is an integration constant and X_{31} is the steady state probability of X_3 :

$$X_{31} \equiv \varepsilon k_2 / \lambda_2 = \frac{K_1 S K_2}{1 + K_0 D + K_1 S (1 + K_2)} \equiv \sigma \quad (52)$$

Other steady state probabilities are:

$$X_{21} = \sigma / K_2, \quad X_{11} = \sigma / K_1 S K_2, \quad X_{01} = \sigma K_0 D / K_1 S K_2$$

Therefore, Scheme 6 includes an exponential process with an apparent rate constant λ_2 , as defined by Eq. 50. λ_2 decreases hyperbolically as D is increased. Fitting the data from the ADP study in rabbit psoas fibers at 20°C to Eq. 50 led us to deduce that $K_0 = 2.8 \text{ mM}^{-1}$ (Kawai and Halvorson 1989) (Table 2). In comparison, solution studies of S1 performed at 20–23°C yielded $K_0 = 3.7 \text{ mM}^{-1}$ (Bagshaw et al. 1974). K_0 is least important among all kinetic constants, however, because D is minimal (0.01–0.02 mM) in the presence of CP/CK (Meyers et al. 1985). Hence $X_0 < 0.01$ and few cross-bridges are distributed in the AMD state.

The above discussion makes it clear that \mathbf{X}_0 , \mathbf{X}_1 and \mathbf{X}_2 correspond to state **A** in Scheme 3, and that \mathbf{X}_3 corresponds to state **B** in Scheme 3. Specifically, \mathbf{X}_1 corresponds to AM (A = actin, M = myosin), to which no nucleotide is bound. \mathbf{X}_2 corresponds to AM*ATP, and \mathbf{X}_0 to AM.ADP. \mathbf{X}_3 corresponds to both the weakly attached AM.ATP and the detached M.ATP. Recently, Palmer et al. (2007) showed a cross-bridge model in which $2\pi c$ corresponds to the detachment step ($\mathbf{X}_2 \leftrightarrow \mathbf{X}_3$ interconversion), based on the stochastic attachment and detachment cycle of cross-bridges.

13 Phosphate release step with a conformational change

Assuming that a cross-bridge state \mathbf{X}_4 makes a conformational change to generate state \mathbf{X}_5 , then the phosphate (**P**) is released to result in state \mathbf{X}_6 (Scheme 7):

If this reaction is viewed in the opposite direction, it follows that **P** forms a collision complex with \mathbf{X}_6 to result in \mathbf{X}_5 , and that \mathbf{X}_5 makes a slow conformational change to result in \mathbf{X}_4 . Mathematically this situation is exactly the same as that described in Scheme 5, with the following substitutions (but not correlations): \mathbf{X}_6 in place of \mathbf{X}_1 , \mathbf{X}_5 in place of \mathbf{X}_2 , \mathbf{X}_4 in place of \mathbf{X}_3 , **P** in place of **S**, K_5 in place of K_1 , k_{-4} in place of k_2 , and k_4 in place of k_{-2} . Therefore, Eq. 44 allows us to derive the apparent rate constant of Scheme 7 as:

$$\lambda_3 = k_4 + \frac{K_5 P}{1 + K_5 P} k_{-4} \quad (53)$$

where P is the Pi concentration, and K_5 is the association constant for **P** to \mathbf{X}_6 . In Scheme 7, K_5 is written underneath the reaction, because the Pi association is the reversal reaction, from \mathbf{X}_6 to \mathbf{X}_5 .

The above discussion makes it clear that \mathbf{X}_4 corresponds to state **B**, and \mathbf{X}_5 and \mathbf{X}_6 to state **C**, of Scheme 3. This assignment cannot be transposed, because from that it would follow that an increase in the Pi concentration results in an increase in force (state **C**), which is opposite to what was observed (Cooke and Pate 1985; Kawai 1986). A transposition of this assignment would also contradict to the previous assignment of the ATP binding step (cross-bridges cycle in the clockwise direction in Scheme 3), because Pi must be released from the cycle. Consequently, \mathbf{X}_4 corresponds to the detached M.ADP.Pi state and the weakly attached AM.ADP.Pi state; \mathbf{X}_5 corresponds to the strongly attached AM*ADP.Pi state, and \mathbf{X}_6

corresponds to the AM*ADP state. It must be pointed out here that the AM*ADP state (\mathbf{X}_6) is completely distinct from the AM.ADP state (\mathbf{X}_0), which is consistent to solution studies (Sleep and Hutton 1980).

When examining the Pi effect, there is also a fast reaction to the left of Scheme 7 (step 1 in Scheme 3) that cannot be ignored, based on conclusion 3 above. The analysis is carried out in the same way as in Scheme 4, to result in the apparent rate constant λ_3 (Kawai and Halvorson 1991):

$$\lambda_3 = \sigma k_4 + \frac{K_5 P}{1 + K_5 P} k_{-4} \quad (54)$$

σ is defined in Eq. 52 ($0 < \sigma < 1$). Thus, the apparent rate constant λ_3 ($2\pi b$) increases and saturates with an increase in either S or P , and it decreases with an increase in D . As seen in Eq. 53 or Eq. 54, λ_3 is a hyperbolic function of P , and fitting the data to this hyperbolic function makes it possible to deduce three kinetic constants (k_4 , k_{-4} , K_5). σ of Eq. 52 is obtained from the ATP study, where the $K_0 D$ term can be dropped because D is very small (0.01–0.02 mM) in the presence of CP/CK. Pi is thought to be released via a narrow deep cleft (back door) in S1 (Yount et al. 1995); hence it is not likely that ADP competitively binds to the Pi binding site. An increase in the ADP concentration decreases the rate constant $2\pi b$ (λ_3), but this is via a reduction of σ in Eqs. 52 and 54.

Equations 53 or 54 has been used extensively to analyze cross-bridge kinetics in rabbit skeletal muscle fibers (Fortune et al. 1991; Kawai and Halvorson 1991; Dantzig et al. 1992; Millar and Homsher 1992; Walker et al. 1992; Wang and Kawai 1997; Galler et al. 2005). With sinusoidal analysis, $k_4 = 56 \text{ s}^{-1}$, $k_{-4} = 129 \text{ s}^{-1}$, and $K_5 = 0.069 \text{ mM}^{-1}$ were deduced for rabbit psoas fibers at 20°C (Kawai and Halvorson 1991). These values compare with those from caged Pi experiments ($k_4 = 79.2 \text{ s}^{-1}$, $k_{-4} = 114.7 \text{ s}^{-1}$, $K_5 = 0.27 \text{ mM}^{-1}$; Dantzig et al. 1992, 20°C) as well as pressure release experiments ($k_4 \sim 15 \text{ s}^{-1}$, $k_{-4} \sim 36 \text{ s}^{-1}$, $K_5 = 0.255 \text{ mM}^{-1}$ at 12°C: deduced from Fortune et al. 1991; see note b of Table 2 legend), and are summarized in Table 2. If the data of the pressure-release experiment are extrapolated to 20°C using the Q_{10} values reported for k_4 (6.8), k_{-4} (1.6), and K_5 (1.1) (Zhao and Kawai 1994), then $k_4 = 69 \text{ s}^{-1}$, $k_{-4} = 52 \text{ s}^{-1}$, and $K_5 = 0.275 \text{ mM}^{-1}$ will result. If the data of the caged Pi experiment by Walker et al. (1992) (Table 2) are extrapolated to 20°C using the same Q_{10} values, then $k_4 = 70 \text{ s}^{-1}$, $k_{-4} = 145 \text{ s}^{-1}$, and $K_5 = 0.172 \text{ mM}^{-1}$. As seen with these numbers, approximate agreement was achieved based on three different techniques from four laboratories. K_5 deduced from sinusoidal analysis is somewhat ($2.5\text{--}4 \times$) smaller, primarily because Fortune et al. (1991), Dantzig et al. (1992), and Walker et al. (1992) fitted the rate constant results to Eq. 53, whereas Kawai and Halvorson (1991) fitted the Pi dependence data of both rate constant (Eq. 54) and amplitude simultaneously. In slow-twitch fibers of rabbit soleus, Millar and Homsher (1992) found: $k_4 = 1.96 \text{ s}^{-1}$ and the second order Pi binding constant $K_5 k_{-4} = 1.994 \text{ mM}^{-1} \text{ s}^{-1}$ when using caged Pi at 20°C. These numbers compare well to those of Wang and Kawai (1997) in Table 2: $k_4 = 5.7 \text{ s}^{-1}$, $k_{-4} = 4.5 \text{ s}^{-1}$, $K_5 = 0.18 \text{ mM}^{-1}$, hence $K_5 k_{-4} = 0.81 \text{ mM}^{-1} \text{ s}^{-1}$. k_4 is usually larger in our case, because of the inclusion of σ (Eq. 54) that accounts for fast equilibria to the left of Scheme 7. Because Pi released by the photolysis of caged Pi is limited to 2–3 mM, it is difficult to probe the saturation phase using this technique ($K_5 = 0.18 \text{ mM}^{-1}$ indicates that half saturation occurs at 5.5 mM Pi). Although Eq. 54 demonstrates a sensitivity to S through σ , this equation has not been used to deduce K_1 or K_2 because of uncertainties about the ATP cleavage step (step 3), which skinned-fiber studies have not been able to resolve (see Section 14).

Conclusion 6

When the effects of ATP, ADP and Pi are considered, the only model consistent to the Le Châtelier–Brown Principle involves assigning phase 2 to steps surrounding the ATP binding step, and assigning phase 3 to steps surrounding the Pi release step. Consequently, cross-bridges cycle in the clockwise direction in Scheme 3, consuming ATP, generating force, and releasing Pi and ADP. Therefore, the transient force increase in phase 2 that was seen by Huxley and Simmons (1971) following step-length release is not the result of energy transduction (that requires ATP), but of a transient accumulation of the number of cross-bridges in the **A** state (which includes both the AM and AM*ATP species). Phase 2 was not correctly assigned because Huxley and Simmons (1971) used intact fibers, and hence did not examine the effects of ATP or Pi concentration.

14 Combined cross-bridge model

Schemes 6 and 7 are combined to summarize the complete cross-bridge Scheme 8.

Note that the steps are renumbered. These are called “elementary steps” or “fundamental steps” (Gutfreund 1995). In this scheme, states \mathbf{X}_3 and \mathbf{X}_4 are equated and represented as \mathbf{X}_{34} for simplicity. In reality, $\mathbf{X}_3 \leftrightarrow \mathbf{X}_4$ (step 3) corresponds to the ATP cleavage step (Lymn and Taylor 1971; Bagshaw et al. 1974; Xu et al. 2003), which is difficult to resolve in skinned fiber studies as they depend on strongly attached cross-bridges. Therefore, cross-bridge states before and after the cleavage of ATP are merged together and referred to as the **Det** (detached) state. The **Det** state includes both the weakly attached states (AM.ATP, AM.ADP.Pi) and the truly detached states (M.ATP, M.ADP.Pi). Because weakly attached states are based on ionic interactions (Brenner et al. 1982), at 200 mM ionic strength the majority of **Det** consists of truly detached states. An accounting of step 3 is one remaining problem that should be solved by skinned fiber experiments in the coming years. What we know already is that step 3 is not very much slower than $2\pi b$ (λ_3), because if it were slower, then the rate constant $2\pi b$ would not be sensitive to the ATP concentration. Therefore, step 3 cannot be rate-limiting for the entire cross-bridge cycle as once suggested (Stein et al. 1985) based on four-state model of Lymn and Taylor (1971). Based on solution studies, it is known that in fast-twitch muscles at 20°C, k_3 and k_{-3} are on the order of 30–120 s⁻¹ (Bagshaw et al. 1974; Xu et al. 2003). The fact that this is similar to the rate constants of step 4 complicates the problem.

Step 6 is the slowest step in the cycle, and can be considered the “rate-limiting” step. If $k_6 + k_{-6}$ is similar to or faster than $k_4 + k_{-4}$, then it follows that an increase in [MgATP] reduces $2\pi b$ and an increase in [MgADP] increases $2\pi b$, both of which are contrary to the experimental evidence (Kawai 1978, 1986). Therefore, $k_6 + k_{-6} < k_4 + k_{-4}$, which makes step 6 the slowest in the cross-bridge cycle. The product of step 6 can be either \mathbf{X}_0 (as shown in Scheme 8) or can be converted directly to \mathbf{X}_1 by ADP release. Experiments in solution carried out by Sleep and Hutton (1980) indicated that $K_6 \sim 50$ (i.e., $k_{-6} \ll k_6$), and that reversal of the \mathbf{X}_0 state to the \mathbf{X}_6 state is possible (shown in a dashed arrow in Scheme 8). That is, \mathbf{X}_0 is likely to be an intermediate product of the hydrolysis pathway, and a part of the cross-bridge cycle.

An examination of Scheme 8 reveals that collision complex formation is followed by a conformational change in three places: (1) step 1 (ATP binding) to step 2, (2) the reversal of step 5 (Pi binding) to step 4, and (3) the reversal of step 0 (ADP binding) to step 6. The conformational change presumably accompanies a change in the force on a cross-bridge and secures ligand binding. This is consistent with the suggestion from Huxley (1980), that chemical reaction (collision complex formation) and mechanical reaction (conformational change) alternate in the cross-bridge cycle. Because these sequential reactions are difficult to resolve, they are frequently merged together. Therefore, the “Pi release step” may include both steps 4 and 5. In fact, the strongly attached AM*ADP.Pi state was not recognized in solution

studies. Hence, in solution systems the conformational change (step 4) must have been merged together and referred to the “Pi release step”. Similarly, the “ADP release step” may include both steps 6 and 0. It has been often stated that the ADP release step is slow, but what that really means is that the preceding conformational change (step 6) is slow. The ADP release step itself (step 0) is a reversal of collision complex formation and, hence, cannot be slow. Similarly, “ATP binding” may include steps 1 and 2.

For the steady-state calculations, step 0 through step 5 can be approximated by equilibrium, and X_i can be calculated from five equilibrium constants (K_i) as formulated by Eq. 18 of Kawai and Halvorson (1991), except when the Pi concentration becomes small (such as < 2 mM). In this case, X_6 becomes large, increasing the turnover rate $k_6 X_6$, which contributes significantly to the steady-state probability of all X_s , hence calculation of X_i needs k_6 (Section 18) and all other rate constants in Scheme 8. The rate-limiting step (step 6) cannot be approximated by equilibrium, as discussed in Sections 8 and 18 and in conclusion 4.

15 Force generation step, isometric tension, and work performance

Solution studies have shown that the Pi release step accompanies a large reduction in free energy (ΔG°), amounting to $\sim 1/2$ the energy generated by ATP hydrolysis (White and Taylor 1976). Hence, this step is almost irreversible (Sleep and Hutton 1980) (note: $\Delta G^\circ = -RT \log K$, where R is the gas constant and K is the equilibrium constant), requiring 10–100 M Pi for reversal (Taylor 1979). This is why White and Taylor (1976) suggested that the Pi release step is associated with the force generation step. Skinned-fiber studies, in contrast, demonstrated that even at mM levels, Pi can diminish isometric tension (Cooke and Pate 1985; Kawai 1986), which indicates that the Pi release step is reversible. This reversibility has been demonstrated through ^{18}O exchange experiments (Webb et al. 1986), and by equilibrium constant measurements showing that $K_4 = 0.43$ (step 4), and $1/K_5 P \cong 1.8$ (step 5 at 8 mM Pi) based on values listed in Table 2 for rabbit psoas fibers (Kawai and Halvorson 1991). Therefore, $\Delta G_4^\circ = +2.0$ kJ/mole and $\Delta G_5^\circ = -1.5$ kJ/mole, and their absolute values are less than RT ($= 2.44$ kJ/mole), hence there is not much change in the free energy in steps 4 or 5. It is likely that in skinned fibers, the free energy of ATP hydrolysis is stored in the contractile apparatus as elastic (mechanical) energy, which can be sensed as force, and can be readily reversed to chemical energy as the Pi concentration is elevated in the mM range. In the solution system, in contrast, a great deal of the liberated free energy is lost as heat. Hence, such a reaction cannot be reversed.

If we focus on one half sarcomere, isometric tension in this structure can be represented by Eq. 55 (Kawai and Zhao 1993). Because all cross-bridges are arranged mechanically in parallel (Fig. 6), overall tension is their sum of the tension of each.

$$(\text{Tension}) = T_0 X_0 + T_1 X_1 + T_2 X_2 + T_5 X_5 + T_6 X_6 \quad (55)$$

where T_i is tension when all cross-bridges are in state X_i ($X_i = 1$). $T_{34} = 0$, because X_{34} is a state that does not generate or support tension. Other T_i values are deduced by comparing isometric tension with X_i as functions of S , P and D . The results of such comparisons are plotted in Fig. 5, for both rabbit psoas fibers (Kawai and Zhao 1993) and soleus slow-twitch fibers (Wang and Kawai 1997). The formulation of Eq. 55 does not change if two half sarcomeres are added serially to make a full sarcomere, assuming that both halves behave in the same way. Similarly, the formulation does not change if many sarcomeres are added in series. If many of these units are added in parallel to make a muscle fiber, then force increases in proportion to the cross-sectional area (A_C). Tension, on the other hand, remains the same because: $(\text{Tension}) = (\text{Force})/A_C$.

\mathbf{X}_5 (AM*ADP.Pi) is a collision complex between \mathbf{P} and \mathbf{X}_6 (AM*ADP). Tension supported (or generated) by \mathbf{X}_5 and \mathbf{X}_6 must be the same, i.e., $T_5 = T_6$ because the conformation of a protein (or proteins) cannot change instantly as the collision complex is formed. If the conformation is the same, the tension must be the same. Because $T_{34} = 0$, force must be generated at step 4, with the transition of \mathbf{X}_{34} to \mathbf{X}_5 . Experimental evidence in support of this insight comes from an evaluation of force as the function of the Pi concentration (Fig. 5) (Kawai and Halvorson 1991; Kawai and Zhao 1993; Wang and Kawai 1997; Ranatunga 1999; Tesi et al. 2002); force does not suddenly decrease as Pi is bound to cross-bridges (Dantzig et al. 1992; Takagi et al. 2004). If additional force is generated upon ADP release, as reported in the case of smooth muscles (Rosenfeld et al. 2001), then it follows that $T_6 < T_0$, $T_0 < T_1$, or $T_6 < T_1$. However, there is no evidence for this in skeletal muscle fiber studies as shown in Fig. 5.

An examination of Fig. 5 shows that forces supported by AM.ADP and AM are not significantly different ($T_0 \approx T_1$). This observation demonstrates that AM.ADP is indeed the collision complex. However, force supported by AM*ATP is significantly less than that supported by AM, indicating that a conformational change may occur by the time AM*ATP is formed. This supposition is strengthened by the finding of yet another state $\text{AM}^\dagger\text{ATP}(\mathbf{X}_{1b})$ between the AM and AM*ATP states, as discussed in Section 16 below. In this case, the tension data as a function of S fit well to the model if we assume that $T_1 = T_{1b}$ (Kawai and Zhao 1994; Wang and Kawai 1997).

In parallel to force generation at step 4 and the transduction of chemical energy into elastic (mechanical) energy, the series compliance (including cross-bridge compliance) is strained. This must be the point of the cross-bridge cycle at which a swing of the lever arm (Dominguez et al. 1998; Geeves and Holmes 1999; Cooke 2005) takes place. Once force is generated, the cross-bridge is stabilized in this conformation by Pi release to result in \mathbf{X}_6 . The contractile system is now ready to perform external work. For this, it is convenient that the next step (step 6) is slow, as the muscle has to transfer both the mechanical energy and the momentum to the load before/while lifting it. The momentum is calculated according to Eq. 56 and related to the force application $F(t)$ and its duration Δt :

$$(\text{momentum}) = (\text{mass}) \times (\text{velocity}) = \int_{\Delta t} F(t) dt = F_{av} \Delta t \quad (56)$$

where F_{av} is the average force. Equation 56 represents a quantity known as the “force-time integral” among muscle physiologists. This equation shows that the momentum increases with increased duration (Δt) of force application. Therefore, the longer the duration, the less force is needed to generate the same amount of momentum. Consequently, the slowest step 6 in the cross-bridge cycle is the most convenient and advantageous place to perform the work (Kawai and Zhao 1993). Figure 5 shows that force progressively decreases as a cross-bridge transitions from \mathbf{X}_6 to \mathbf{X}_0 to \mathbf{X}_1 to \mathbf{X}_2 and as external work is performed. As is clear from the above discussion, “force generation” and “work performance” are two different entities, although the term “power stroke” is often used interchangeably in referring to each. It would be highly desirable that future publications clearly distinguish between these two distinct concepts.

16 Exponential process D and one extra cross-bridge state

In some of our publications on rabbit psoas fibers (e.g., Kawai and Zhao 1993; Zhao and Kawai 1994) as well as soleus slow-twitch fibers (Wang and Kawai 1996, 1997) and on myocardium (Kawai et al. 1993; Zhao and Kawai 1996), an extra exponential process (termed process D) that occurs at higher frequency than process C ($2\pi d > 2\pi c$) was described. Similarly, in the case of phase 2 of step analysis, Abbott and Steiger (1977), Coupland et al. (2001), and Davis et al.

(2002) resolved two exponential processes in rabbit psoas fibers, and Ford et al. (1977) recognized four exponential processes in frog tibialis anterior fibers. Because of the ATP dependence of process D, we ascribed this process to an extra step that occurs immediately after ATP binding to the myosin head as in Scheme 9:

where X_{1b} is the collision complex, step 1b is a conformational change, and step 2 is yet another conformational change. X_{1b} corresponds to $AM^{\dagger}ATP$, X_2 to AM^*ATP and X_3 to $AM.ATP$. Processes D and C appear to be better separated in slow-twitch fibers (Wang and Kawai 1996, 1997) and in myocardium (Kawai et al. 1993) than in fast-twitch fibers. The rate constants of step 1b are entered in Table 2 where available. While it is entirely possible that process D corresponds to the extra step in the cross-bridge cycle that is shown in Scheme 9, we have not performed this analysis in recent publications, primarily because the cross-bridge scheme and associated math become more complex, and we do not wish to over interpret our results. We have been using phenomenological correlations between observed exponential processes and the elementary steps among various muscle preparations (the columns in Table 2), but this correlation may differ depending on which muscle type being tested, in particular in the case of slow-twitch fibers and in myocardium. It is possible that the process D becomes more important in slow-twitch fibers and in myocardium than in fast-twitch fibers.

17 Stiffness

Stiffness depends on the number of attached cross-bridges as well as on series compliance (Huxley et al. 1994; Wakabayashi et al. 1994; Kojima et al. 1994; Higuchi et al. 1995) and parallel stiffness (Fig. 6). Because these elements are intermixed and distributed, the formal mathematical treatment becomes extremely complex, as was shown by Mijailovich et al. (1996). The particular patterns in which cross-bridges are arrayed and linked to thin filaments add another degree of complexity with respect to determining the relationship between the force of individual cross-bridges and measured stiffness or tension (Tanner et al. 2007). For practical applications, however, we have previously proposed a simple model in which a parallel array of attached cross-bridges “y” is connected to a series compliance q (Fig. 6) (Wang and Kawai 1997; Kawai 2003), and the entire structure is connected to parallel stiffness S_p . Both series compliance and the parallel stiffness can have viscous components at the same time. Hence, in general, q and S_p are frequency-dependent, complex numbers. In this model:

$$(\text{Stiffness})=Y_a X_a / (1 + Y_a X_a q) + S_p \quad (57)$$

$$\text{where } X_a \equiv X_0 + X_1 + X_2 + X_5 + X_6 = 1 - X_{34}$$

and Y_a is the stiffness contribution from the cross-bridges when all cross-bridges are attached ($X_a = 1$). The contribution of the parallel stiffness can be removed by subtraction of the viscoelasticity of a muscle fiber when all cross-bridges are detached (when \otimes is open in Fig. 6). Classically, S_p would be the viscoelasticity of relaxed muscle fibers. However, it may be better to measure this quantity on fibers that are relaxed by using 40 mM 2,3- butanedione monoxime (BDM) (e.g., Fujita et al. 2002) in the presence of Ca^{2+} in new experiments, because the property of connectin (titin) has been reported to change once Ca^{2+} is bound to it (Labeit et al. 2003). Connectin, residual sarcolemma, and collagen in the extra cellular matrix contribute most to parallel stiffness. In rabbit psoas fibers at a sarcomere length of 2.5 μm , S_p is small and almost negligible (Kawai and Brandt 1980) making parallel stiffness a minor consideration. Because Eq. 57 approaches $1/q + S_p$ as X_a becomes large, stiffness cannot be used to index the number of attached cross-bridges as is the case for the high temperature range

in rabbit psoas fibers (Kawai 2003). When X_a is small, stiffness can be used to index the number of attached cross-bridges. In this case, Eq. 57 becomes $Y_a X_a + S_P$.

18 ATP hydrolysis rate and the rate constant of step 6

The formula for calculation of the ATP hydrolysis rate can be derived from Eq. 40 (Zhao and Kawai 1994):

$$J=(\text{ATPase})=A_T(k_6 X_6 - k_{-6} X_0) \cong A_T k_6 X_6 \quad (58)$$

In practice, the k_{-6} term is dropped as shown, both because this reaction is highly unidirectional ($K_6 \sim 50$, hence $k_6 \gg k_{-6}$; Sleep and Hutton 1980) and due to the fact that X_0 is very small (<0.01) under normal experimental conditions in which the ADP concentration is 0.01–0.02 mM in the presence of CP/CK. A_T is the total myosin S1 concentration, and it is 0.17–0.2 mM in psoas fibers (Yates and Greaser 1983; Tikunov et al. 2000), 0.13–0.14 mM in soleus fibers (Tikunov et al. 2000), and 0.15 mM in myocardium (Barsotti and Ferenczi 1988). $k_6 = 16\text{--}18 \text{ s}^{-1}$ was deduced using Eq. 58 and data from the ATP hydrolysis rate in rabbit psoas fibers at 15–20°C (Zhao and Kawai 1994).

19 Series compliance, force development, and the slowest step in the cross-bridge cycle

As discussed in Section 17, series compliance makes an important contribution on muscle mechanics (Huxley et al. 1994; Wakabayashi et al. 1994; Kojima et al. 1994; Higuchi et al. 1995; Wang et al. 1999; Kawai 2003). This is particularly evident at the onset of contraction, when force develops from a zero load to the maximum load. In the following, we define that η is the step size, v is the number of steps that take place in 1 sec, and ρ' is the stiffness of one half sarcomere, which includes the contribution from both series compliance and cross-bridges (Eq. 57). For simplicity, we assume that $S_P = 0$. Under isometric conditions, the increase in force (dF) during dt is:

$$dF = \rho' \eta v dt \quad (59)$$

In Eq. 59, ηv is the distance in 1 sec to pull the thin filament toward the M-line (hence ηv is the velocity of filament elongation), which at the same time stretches series compliance and other compliant elements of cross-bridges to result in a force increase by $\rho' (\eta v)$. Let us assume that developed force (F) affects η in the following way:

$$\eta = \eta_0 (1 - F/F_0) \quad (60)$$

where F_0 is the maximum isometric force. That is, a step of the cross-bridge becomes increasingly more difficult as force develops, and as discussed by Piazzesi et al. (2007). Equation 60 can be actually derived from the force–velocity relationship (see e.g., Woledge et al. 1985; Debold et al. 2005) by a linear extrapolation of the velocity at F_0 . An alternative to Eq. 60 can be generated if we assume that:

$$v = v_0 (1 - F/F_0) \quad (61)$$

Equation 61 is an expression of the Fenn effect (Fenn 1923), i.e. the rate of stepping becomes increasingly more difficult as force develops. From Eq. 59 and Eq. 60 (or Eq. 61), we get:

$$dF/dt + \lambda_4 F = \lambda_4 F_0 \quad (62)$$

$$\text{where } \lambda_4 \equiv \rho' \eta_0 v_0 / F_0 \quad (63)$$

$$\text{Therefore, } F_0 / \rho' = \eta_0 v_0 / \lambda_4 \quad (64)$$

Thus, from Eq. 62 (Appendix 1) we arrive at:

$$F(t) = F_0 [1 - \exp(-\lambda_4 t)] \quad (65)$$

This system has one exponential process with an apparent rate constant of λ_4 and amplitude F_0 . Note that $F(0) = 0$ is assumed. Equation 65 would be the form of a force time course in which a fiber is suddenly activated by Ca^{2+} , or in which the length of the active fiber is suddenly released to zero load and restretched to its original length (resulting in force redevelopment like that seen by k_{tr} measurement). The exponential function (Eq. 65) may be a good approximation for describing the time course data. In fact, available data are consistent with the exponential function (e.g. Regnier et al. 1995; Stehle et al. 2002; Piroddi et al. 2003).

Now, let us evaluate the right side of Eq. 64. With single myofibrils, Piroddi et al. (2003) observed $k_{tr} = 8.0 \text{ s}^{-1}$ and $k_{act} = 7.9 \text{ s}^{-1}$ in rabbit psoas at 15°C . These are the values of λ_4 . $1/v_0$ is the average time a cross-bridge spends for one cycle, and is related to the elementary steps by:

$$\frac{1}{v_0} = \frac{1}{\lambda_2} + \frac{1}{\lambda_3} + \frac{1}{k_6 + k_{-6}} \quad (66)$$

In Eq. 66, each term on the right-hand side corresponds to a time constant: $1/\lambda_2$ is the time constant of step 2, which is the average time a cross-bridge spends to complete step 2; similarly, $1/\lambda_3$ is the average time spent to complete step 4, and $1/(k_6 + k_{-6})$ is the average time spent to complete step 6. If $k_6 \ll \lambda_3$ (note that: $k_{-6} \ll k_6$, $\lambda_3 < \lambda_2$), then from Eq. 66,

$$v_0 \cong k_6 \quad (67)$$

$k_6 \cong 16\text{--}18 \text{ s}^{-1}$ was reported in rabbit psoas fibers at $15\text{--}20^\circ\text{C}$ (Zhao and Kawai 1994); hence $v_0 \sim 17 \text{ s}^{-1}$. $\eta_0 = 5.3 \text{ nm}$ was reported by Kitamura et al. (1999) for the step size (see also Molloy et al. 1995; Guilford et al. 1997). Thus, the right side of Eq. 64 is:

$$\eta_0 v_0 / \lambda_4 = 5.3 \text{ nm} \times 17 \text{ s}^{-1} / 7.95 \text{ s}^{-1} = 11 \text{ nm}$$

The left side of Eq. 64 (F_0 / ρ') is the same as the (force):(stiffness) ratio, or the instantaneous length release needed to abolish full tension. The ratio (active tension):(elastic modulus) was measured to be $T:Y_\infty = 1.14\%$ in rabbit psoas fibers at 15°C (Zhao and Kawai 1994). Therefore,

$$(\text{Force})/(\text{stiffness})=1.25 \mu\text{m} \times 0.0114=14 \text{ nm}$$

where 1.25 μm is the half sarcomere length of the experiment. Thus, approximate agreement can be reached for both sides of Eq. 64, which may validate this equation and the theory behind it. Because k_{tr} is slowest of all rate constants measured in the cross-bridge cycle, this parameter has been thought to be limited by the slowest step in the cross-bridge cycle (Gordon et al. 2000). The above analysis provides support for this hypothesis.

The fact that k_{tr} is affected by Pi (Regnier et al. 1995; Tesi et al. 2000) is presumably related to the approximation used in Eq. 67, which can be improved by inclusion of the Pi effect (λ_3 is affected by the Pi concentration: Eq. 54). Assuming that the $1/\lambda_2$ term can be ignored in Eq. 66 (because $\lambda_2 \gg k_6$), Eq. 66 can be rewritten by using Eq. 54 to result in Eq. 68.

$$v_0=v_{00}+\frac{\psi K_5 P}{1+\xi K_5 P} \quad (68)$$

$$\text{where } v_{00} \equiv \frac{\sigma k_4 k_6}{\sigma k_4 + k_6} = k_6 - \frac{k_6^2}{\sigma k_4 + k_6} \quad (69)$$

$$\text{and } \psi \equiv \frac{k_{-4} k_6^2}{(\sigma k_4 + k_6)^2}, \quad \xi \equiv 1 + \frac{k_{-4}}{\sigma k_4 + k_6} \quad (70)$$

Equation 68 is a hyperbolically increasing and saturating function with respect to P , which is similar to Eqs. 53 and 54. Thus, an increase in P results in the increase in λ_4 via Eq. 63 and as reported (Regnier et al. 1995; Tesi et al. 2000). Similarly, an increase in S results in the increase in λ_4 via $S \rightarrow \sigma \rightarrow \lambda_3 \rightarrow v_0 \rightarrow \lambda_4$ (see Eqs. 52, 54, 66, 63, respectively).

Several colleagues in the field have suggested that exponential process A of sinusoidal analysis (and hence phase 4 of step analysis) may represent the slowest step of the cross-bridge cycle (step 3 in Scheme 3, and step 6 in Scheme 8). Until recently, we have discounted this possibility because the three-state model, as represented in Scheme 3, can have only two exponential processes (see Appendix 2 for an analysis of a general case) and, in principle, the rate constants of the slowest step cannot be detected by the perturbation analysis method. The same is true for Scheme 8. However, the introduction of series compliance changes this outlook significantly. As shown above, series compliance may introduce an extra exponential process with a slow rate constant, such as $2\pi a$ of process A, which is present in all three subtypes of fast-twitch muscle fibers examined (Galler et al. 2005). In contrast, the amplitude of process A (phase 4) is very small or even absent in the cases of insect indirect flight muscles (Fig. 3) (Thorson and White 1969; Abbott 1973; Pringle 1978; Marcussen and Kawai 1990; Swank et al. 2006), myocardium (Saeki et al. 1978, 1991; Zhao and Kawai 1996; Wannenburg et al. 2000; Fujita et al. 2002), and covalently but partially cross-linked rabbit psoas fibers (Tawada and Kawai 1990). In slow-twitch fibers, process A is present but its amplitude is small (Kawai and Schachat 1984; Wang and Kawai 1996, 1997). These observations suggest that the sarcomere structure is more rigid in these muscle preparations than in fast-twitch skeletal muscle fibers, minimizing the amplitude of process A. In fact, in insect muscle fibers, an extra C-filament is present to secure the connection between the thick filament and the Z-line, and

to stabilize the sarcomere structure (White 1983). In cardiac muscles, there is a possibility that myosin binding protein C (MyBP-C) reaches the thin filament (Spirito et al. 1997; Squire et al. 2003), which may give extra stability to sarcomeres. In partially cross-linked rabbit psoas fibers, the extra covalent linkage (18% of cross-bridges) was created to stabilize the preparation, causing process A to disappear (Tawada and Kawai 1990).

Let us perform a calculation to examine the possibility that process A (phase 4) represents the slowest step of the cross-bridge cycle. Because $2\pi a = 6 \text{ s}^{-1}$ was observed in rabbit psoas fibers at 20°C (Zhao and Kawai 1994), the right side of Eq. 64 becomes:

$$\eta_0 v_0 / \lambda_4 = 5.3 \text{ nm} \times 17 \text{ s}^{-1} / 6 \text{ s}^{-1} = 15 \text{ nm}$$

Because $T:Y_\infty = 1.3\%$ was observed in the same study (20°C), the left side of Eq. 64 becomes:

$$(\text{Force})/(\text{stiffness}) = 1.25 \text{ } \mu\text{m} \times 0.013 = 16 \text{ nm}$$

Thus, the values are consistent with process A being the slowest step of the cross-bridge cycle. This insight is, however, limited to preparations in which process A (phase 4) can be observed. In any case, this is a subject that will be exciting to pursue in future studies.

Conclusion 7

The apparent rate constant of tension development (k_{act} , k_{tr}) or of process A of sinusoidal analysis (phase 4 of step analysis) appears to be proportionate to the rate constant of the slowest step of the cross-bridge cycle (k_6), with the proportionality constant $\rho' \eta_0 / F_0$ (Eq. 63). This proportionality exists because of the presence of in-series compliance in sarcomeres.

20 More realistic conditions

In the discussion in Sections 7–18, the condition ($\alpha + \alpha' \gg \beta + \beta' \gg \gamma + \gamma'$) was used for the sake of simplicity. However, what would happen if this condition were not met, and if the conditions were merely $\alpha + \alpha' > \beta + \beta' > \gamma + \gamma'$ as suggested from the kinetic constants listed in Table 2? The answer to this question is simply that the approximation becomes less accurate as these numbers get closer to each other, and that the analysis may become qualitative rather than quantitative. That is, there will be an increasing contribution of steps 4–5 to the apparent rate constant λ_2 of phase 2, with the Pi concentration consequently having increasingly more influence on phase 2. The conclusions derived then become qualitative, and their usefulness depends on one's own expectations. They include the assignment of phase 2 and its rate constant λ_2 to step 2 of Scheme 8, and the assignment of phase 3 and its rate constant λ_3 to step 4 of the same scheme. If, however, one is not satisfied with this approximation, then an exact derivation can be undertaken according to Appendix 2. Alternatively, one could use the method used to analyze the data from experiments in myocardium (Section 21), as this does not rely on approximation.

21 Cardiac muscle fibers

In cardiac muscle fibers (myocardium), the apparent rate constants λ_2 ($2\pi c$) and λ_3 ($2\pi b$) are closer to one another than their counterparts in skeletal muscle fibers are, and thus the approximation approach is not as accurate as in skeletal fibers. In fact, we have found that the Pi concentration affects the apparent rate constant $2\pi c$ significantly. In this case, the sum (Eq. 71) and the product (Eq. 72) of the two apparent rate constants can be used to deduce the kinetic constants of the elementary steps. If we take this approach, there is no need for approximation

except that we still have to assume that k_6 is much smaller (\ll) than other rate constants. Under these conditions,

$$\lambda_2 + \lambda_3 = \varepsilon k_2 + k_{-2} + k_4 + \zeta k_{-4} \quad (71)$$

$$\lambda_2 \lambda_3 = \varepsilon k_2 k_4 + \varepsilon \zeta k_2 k_{-4} + \zeta k_{-2} k_{-4} \quad (72)$$

$$\text{where } \zeta \equiv K_5 P / (1 + K_5 P) \quad (73)$$

ε is defined in Eq. 49 [$\varepsilon = K_1 S / (1 + K_0 D + K_1 S)$]. For the derivation of Eqs. 71 and 72, see Eqs. 14 and 15 of Kawai and Halvorson (1991). Both Eqs. 71 and 72 are hyperbolic functions of S , P and D , as are the previously discussed Eqs. 50 and 54. By fitting the data (effects of S , P and D) to these equations, we can deduce all rate constants (k_2 , k_{-2} , k_4 , k_{-4}) and association constants (K_0 , K_1 , K_5). This method enabled us to resolve the kinetic constants of the elementary steps in ferret myocardium (Kawai et al. 1993) and bovine myocardium (Lu et al. 2005).

Martin and Barsotti (1994) used caged ATP on guinea pig heart muscle, and deduced the second order ATP binding constant (our $K_1 k_2$) to be $\sim 39 \text{ mM}^{-1} \text{ s}^{-1}$ at 21°C . This number compares with the values we have calculated from Table 2: ferret myocardium $48 \text{ mM}^{-1} \text{ s}^{-1}$ (2°C , Kawai et al. 1993), porcine myocardium $138 \text{ mM}^{-1} \text{ s}^{-1}$ (20°C , Zhao and Kawai 1996), and bovine myocardium $240 \text{ mM}^{-1} \text{ s}^{-1}$ (25°C , Fujita et al. 2002). Araujo and Walker (1996) used caged Pi on rat ventricular myocytes, and found the second order Pi binding constant (our $K_5 k_{-4}$) to be $3.1 \text{ mM}^{-1} \text{ s}^{-1}$ (15°C). This number compares well with our values calculated from Table 2 (same references): ferret myocardium $6.4 \text{ mM}^{-1} \text{ s}^{-1}$ (20°C), porcine myocardium $1.1 \text{ mM}^{-1} \text{ s}^{-1}$ (20°C), and bovine myocardium $1.8 \text{ mM}^{-1} \text{ s}^{-1}$ (25°C). Thus, even when very different techniques and different cardiac preparations are used, we are able to achieve approximate agreement.

22 Conclusion and future direction

As shown in this mini review, the three-state model is adequate to account for the three phases of force transients that are generated in response to a step length change. The six-state model is an extension of the three-state model that includes ligand (ATP, ADP, Pi)-bound states. In order to correlate each phase of a transient to individual elementary step of the cross-bridge cycle correctly, it is necessary to examine the effects of these ligand concentrations on the apparent rate constants and to fit their results to the model. Therefore, any future cross-bridge models must be able to predict the effects of these ligands, in particular those of ATP and Pi. When studying force transients, it is best not to make a large increase in force, because this may cause a delay in the time course to stretch series elastic elements. Since multiple cross-bridge cycles are needed to stretch series elastic elements, the time course may be limited by the slowest step (rate-limiting step) of the cross-bridge cycle (Section 19).

Acknowledgments

The authors are indebted to Dr. David W. Maughan of the University of Vermont (USA) for his critical reading of the manuscript and his constructive comments and useful suggestions. The authors are also grateful to Dr. Christine Blaumueller for her critical reading of the manuscript and creative suggestions. This work was supported by a grant from NIH HL70041 to MK. The contents of this work are solely the responsibility of the authors and do not necessarily represent the official view of the awarding organization.

References

- Abbott RH. An interpretation of the effect of fiber length and calcium on the mechanical properties of insect flight muscle. *Cold Spring Harb Symp Quant Biol* 1973;37:647–654.
- Abbott RH, Steiger GJ. Temperature and amplitude dependence of tension transients in glycerinated skeletal and insect fibrillar muscle. *J Physiol* 1977;266:13–42. [PubMed: 856995]
- Araujo A, Walker JW. Phosphate release and force generation in cardiac myocytes investigated with caged phosphate and caged calcium. *Biophys J* 1996;70:2316–2326. [PubMed: 9172755]
- Bagni MA, Cecchi G, Colomo F, Poggese C. Tension and stiffness of frog muscle fibres at full filament overlap. *J Muscle Res Cell Motil* 1990;11:371–377. [PubMed: 2266164]
- Bagshaw CR, Eccleston JF, Eckstein F, Goody RS, Gutfreund H, Trentham DR. The magnesium ion-dependent adenosine triphosphatase of myosin. Two-step processes of adenosine triphosphate association and adenosine diphosphate dissociation. *Biochem J* 1974;141:351–364. [PubMed: 4281654]
- Barsotti RJ, Ferenczi MA. Kinetics of ATP hydrolysis and tension production in skinned cardiac muscle of the guinea pig. *J Biol Chem* 1988;263:16750–16756. [PubMed: 3182811]
- Bershtsky SY, Tsaturyan AK. Tension responses to joule temperature jump in skinned rabbit muscle fibres. *J Physiol* 1992;447:425–448. [PubMed: 1593453]
- Brenner B. Effect of Ca^{2+} on cross-bridge turnover kinetics in skinned single rabbit psoas fibers: implications for regulation of muscle contraction. *Proc Natl Acad Sci USA* 1988;85:3265–3269. [PubMed: 2966401]
- Brenner B, Schoenberg M, Chalovich JM, Greene LE, Eisenberg E. Evidence for cross-bridge attachment in relaxed muscle at low ionic strength. *Proc Natl Acad Sci USA* 1982;79:7288–7291. [PubMed: 6961408]
- Burton K, Simmons RM, Sleep J. Kinetics of force recovery following length changes in active skinned single fibres from rabbit psoas muscle. *J Physiol* 2006;573(2):305–328. [PubMed: 16497718]
- Campbell KB, Razumova MV, Kirkpatrick RD, Slinker BK. Nonlinear myofilament regulatory processes affect frequency-dependent muscle fiber stiffness. *Biophys J* 2001;81:2278–2296. [PubMed: 11566798]
- Cooke R. Milestone in physiology: the sliding filament model: 1972–2004. *J Gen Physiol* 2005;123:643–656. [PubMed: 15173218]
- Cooke R, Pate E. The effects of ADP and phosphate on the contraction of muscle fibers. *Biophys J* 1985;48:789–798. [PubMed: 3878160]
- Coupland ME, Puchert E, Ranatunga KW. Temperature dependence of active tension in mammalian (rabbit psoas) muscle fibres: effect of inorganic phosphate. *J Physiol* 2001;536:879–891. [PubMed: 11691880]
- Dantzig J, Goldman Y, Millar NC, Laktis J, Homsher E. Reversal of the cross-bridge force-generating transition by the photogeneration of phosphate in rabbit psoas muscle fibers. *J Physiol* 1992;451:247–278. [PubMed: 1403812]
- Davis JS, Rodgers ME. Force generation and temperature-jump and length-jump tension transients in muscle fibers. *Biophys J* 1995;68:2032–2040. [PubMed: 7612845]
- Davis JS, Satorius CL, Epstein ND. Kinetic effects of myosin regulatory light chain phosphorylation on skeletal muscle contraction. *Biophys J* 2002;83:359–370. [PubMed: 12080126]
- Dickinson MH, Hyatt CJ, Lehmann F-O, Moore JR, Reedy MC, Simcox A, Tohtong R, Vigoreaux JO, Yamashita H, Maughan DW. Phosphorylation-dependent power output of transgenic flies: an integrated study. *Biophys J* 1997;73:3122–3134. [PubMed: 9414224]
- Dobbie I, Linari M, Piazzesi G, Reconditi M, Koubassova N, Ferenczi M, Lombardi V, Irving M. Elastic bending and active tilting of myosin heads during muscle contraction. *Nature* 1998;396:383–387. [PubMed: 9845077]
- Dominguez R, Freyzon Y, Trybus KM, Cohen C. Crystal structure of a vertebrate smooth muscle myosin motor domain and its complex with the essential light chain: visualisation of the pre-power stroke state. *Cell* 1998;94:559–571. [PubMed: 9741621]
- Fenn WO. A quantitative comparison between the energy liberated and the work performed by the isolated sartorius muscle of the frog. *J Physiol* 1923;58:175–203. [PubMed: 16993652]

- Finer JT, Simmons RM, Spudich JA. Single myosin mechanics: piconewton forces and nanometre steps. *Nature (Lond)* 1994;368:113–119. [PubMed: 8139653]
- Ford LE, Huxley AF, Simmons RM. Tension responses to sudden length change in stimulated frog muscle fibres near slack length. *J Physiol* 1977;269:441–515. [PubMed: 302333]
- Fortune NS, Geeves MA, Ranatunga KW. Tension responses to rapid pressure release in glycerinated rabbit muscle fibers. *Proc Natl Acad Sci USA* 1991;88:7323–7327. [PubMed: 1871140]
- Fujita H, Sasaki D, Ishiwata S, Kawai M. Elementary steps of the cross-bridge cycle in bovine myocardium with and without regulatory proteins. *Biophys J* 2002;82:915–928. [PubMed: 11806933]
- Galler S, Wang BG, Kawai M. Elementary steps of the cross-bridge cycle in fast-twitch fiber types from rabbit skeletal muscles. *Biophys J* 2005;89:3248–3260. [PubMed: 16143633]
- Geeves MA, Holmes KC. Structural mechanism of muscle contraction. *Annu Rev Biochem* 1999;68:687–728. [PubMed: 10872464]
- Geeves MA, Holmes KC. The molecular mechanism of muscle contraction. *Adv Protein Chem* 2005;71:161–193. [PubMed: 16230112]
- Goldman YE, Hibberd MG, Trentham DR. Relaxation of rabbit psoas muscle fibres from rigor by photochemical generation of adenosine-5'-triphosphate. *J Physiol* 1984;354:577–604. [PubMed: 6481645]
- Gordon AM, Homsher E, Regnier M. Regulation of contraction in striated muscle. *Physiol Rev* 2000;80:853–924. [PubMed: 10747208]
- Guilford WH, Dupuis DE, Kennedy G, Wu J, Patlak JB, Warshaw DM. Smooth muscle and skeletal muscle myosins produce similar unitary forces and displacements in the laser trap. *Biophys J* 1997;72:1006–1021. [PubMed: 9138552]
- Gutfreund, H. Receptors, transmitters and catalysts. Cambridge University Press; 1995. Kinetics for the life sciences.
- Heinl P, Kuhn HJ, Rüegg JC. Tension responses to quick length changes of glycerinated skeletal muscle fibres from the frog and tortoise. *J Physiol* 1974;237:243–258. [PubMed: 4545181]
- Herrmann C, Lionne C, Travers F, Barman T. Correlation of ActoS1, myofibrillar, and muscle fiber ATPases. *Biochemistry* 1994;33:4148–4154. [PubMed: 8155632]
- Higuchi H, Yanagida T, Goldman YE. Compliance of thin filaments in skinned fibers of rabbit skeletal muscle. *Biophys J* 1995;69:1000–1010. [PubMed: 8519955]
- Homsher W, Millar NC. Caged compounds and striated muscle contraction. *Annu Rev Physiol* 1990;52:875–896. [PubMed: 2139560]
- Huxley AF. Muscle structure and theories of contraction. *Prog Biophys Biophys Chem* 1957;7:255–318. [PubMed: 13485191]
- Huxley AF. Muscular contraction. *J Physiol* 1974;243:1–43. [PubMed: 4449057]
- Huxley, AF. Reflections on muscle. Princeton University Press; Princeton: 1980.
- Huxley AF, Simmons RM. Proposed mechanism of force generation in striated muscle. *Nature* 1971;233:533–538. [PubMed: 4939977]
- Huxley HE, Stewart A, Sosa H, Irving T. X-ray diffraction measurements of the extensibility of actin and myosin filaments in contracting muscle. *Biophys J* 1994;67:2411–2421. [PubMed: 7696481]
- Ishijima A, Kojima H, Higuchi H, Harada Y, Funatsu T, Yanagida T. Multiple- and single-molecule analysis of the actomyosin motor by nanometer-piconewton manipulation with a microneedle: unitary steps and force. *Biophys J* 1996;70:383–400. [PubMed: 8770215]
- Julian FJ, Sollins KR, Sollins MR. A model for the transient and steady-state mechanical behavior of contracting muscle. *Biophys J* 1974;14:546–562. [PubMed: 4836669]
- Kawai M. Head rotation or dissociation? A study of exponential rate processes in chemically skinned rabbit muscle fibers when MgATP concentration is changed. *Biophys J* 1978;22:97–103. [PubMed: 638228]
- Kawai M. The role of orthophosphate in crossbridge kinetics in chemically skinned rabbit psoas fibers as detected with sinusoidal and step length alterations. *J Muscle Res Cell Motil* 1986;7:421–434. [PubMed: 3491834]

- Kawai M. What do we learn by studying the temperature effect on isometric tension and tension transients in mammalian striated muscle fibres? *J Muscle Res Cell Motil* 2003;24:127–138. [PubMed: 14609024]
- Kawai M, Brandt PW. Sinusoidal analysis: a high resolution method for correlating biochemical reactions with physiological processes in activated skeletal muscles of rabbit, frog and crayfish. *J Muscle Res Cell Motil* 1980;1:279–303. [PubMed: 6971874]
- Kawai M, Halvorson HR. Role of MgATP and MgADP in the crossbridge kinetics in chemically skinned rabbit psoas fibers. Study of a fast exponential process (C). *Biophys J* 1989;55:595–603. [PubMed: 2785822]
- Kawai M, Halvorson HR. Two step mechanism of phosphate release and the mechanism of force generation in chemically skinned rabbit psoas muscle. *Biophys J* 1991;59:329–342. [PubMed: 2009356]
- Kawai M, Schachat FH. Differences in the transient response to fast and slow skeletal muscle fibers: correlations between complex modulus and myosin light chains. *Biophys J* 1984;45:1145–1151. [PubMed: 6743745]
- Kawai M, Zhao Y. Cross-bridge scheme and force per cross-bridge state in skinned rabbit psoas muscle fibers. *Biophys J* 1993;65:638–651. [PubMed: 8218893]
- Kawai M, Saeki Y, Zhao Y. Cross-bridge scheme and the kinetic constants of elementary steps deduced from chemically skinned papillary and trabecular muscles of the ferret. *Circ Res* 1993;73:35–50. [PubMed: 8508533]
- Kirkwood, JG.; Oppenheim, I. Chemical thermodynamics. McGraw-Hill Book Co. Inc; New York: 1961.
- Kitamura K, Tokunaga M, Iwane AH, Yanagida T. A single myosin head moves along an actin filament with regular steps of 5.3 nanometres. *Nature* 1999;397(6715):129–134. [PubMed: 9923673]
- Kojima H, Ishijima A, Yanagida T. Direct measurement of stiffness of single actin filaments with and without tropomyosin by in vitro nanomanipulation. *Proc Natl Acad Sci USA* 1994;91:12962–12966. [PubMed: 7809155]
- Labeit D, Watanabe K, Witt C, Fujita H, Wu Y, Lahmers S, Funck T, Labeit S, Granzier H. Calcium-dependent molecular spring elements in the giant protein titin. *Proc Natl Acad Sci* 2003;100:13716–13721. [PubMed: 14593205]
- Lu X, Bryant MK, Bryan KE, Rubenstein PA, Kawai M. Role of the N-terminal negative charge of actin in cross-bridge kinetics and force generation in reconstituted bovine myocardium. *J Physiol* 2005;564(1):65–82. [PubMed: 15649975]
- Lynn RW, Taylor EW. Mechanism of adenosine triphosphate hydrolysis by actomyosin. *Biochemistry* 1971;10:4617–4624. [PubMed: 4258719]
- Marcussen, BL.; Kawai, M. Role of MgATP and inorganic phosphate ions in crossbridge kinetics in insect (*Lethocerus colossicus*) flight muscle. In: Sperlakis, N.; Wood, JD., editors. *Frontiers in smooth muscle research*. Wiley-Liss; New York: 1990. p. 805-813.
- Martin H, Barsotti RJ. Relaxation from rigor of skinned trabeculae of the guinea pig induced by laser photolysis of caged ATP. *Biophys J* 1994;66:1115–1128. [PubMed: 8038383]
- Meyer RA, Brown TR, Kushmerick MJ. Phosphorus nuclear magnetic resonance of fast- and slow-twitch muscle. *Am J Physiol* 1985;248:C279–C287. [PubMed: 3976878]
- Mijailovich SM, Fredberg JJ, Butler JP. On the theory of muscle contraction: filament extensibility and the development of isometric force and stiffness. *Biophys J* 1996;71:1475–1484. [PubMed: 8874021]
- Millar NC, Geeves MA. Protein fluorescence changes associated with ATP and adenosine 5'-[γ -thio] triphosphate binding to skeletal muscle myosin subfragment 1 and actomyosin subfragment 1. *Biochem J* 1988;249:735–743. [PubMed: 3355494]
- Millar NC, Homsher E. Kinetics of force generation and phosphate release in skinned rabbit soleus muscle fibers. *Am J Physiol* 1992;252Cell Physiol 31:C1239–C1245.
- Miyata H, Yoshikawa H, Hakozaki H, Suzuki N, Furuno T, Ikegami A, Kinoshita K Jr, Nishizaka T, Ishiwata S. Mechanical measurements of single actomyosin motor force. *Biophys J* 1995;68:286S–290S. [PubMed: 7787092]
- Molloy JE, Burns JE, Kendrick-Jones J, Tregear RT, White DCS. Movement and force produced by a single myosin head. *Nature (Lond)* 1995;378:209–212. [PubMed: 7477328]

- Murase M, Tanaka H, Nishiyama K, Shimizu H. A three-state model for oscillation in muscle: sinusoidal analysis. *J Muscle Res Cell Motil* 1986;7:2–10. [PubMed: 3958157]
- Palmer BM, Suzuki T, Wang Y, Barnes WD, Miller MS, Maughan DW. Two-state model of acto-myosin attachment-detachment predicts C-process of sinusoidal analysis. *Biophys J* 2007;93:760–769. [PubMed: 17496022]
- Piazzesi G, Reconditi M, Linari M, Lucii L, Bianco P, Brunello E, Decostre V, Stewart A, Gore DB, Irving TC, Irving M, Lombardi V. Skeletal muscle performance determined by modulation of number of myosin motors rather than motor force or stroke size. *Cell* 2007;131:784–795. [PubMed: 18022371]
- Piroddi N, Tesi C, Pellegrino MA, Tobacman LS, Homsher E, Poggesi C. Contractile effects of the exchange of cardiac troponin for fast skeletal troponin in rabbit psoas single myofibrils. *J Physiol* 2003;552.3:917–931. [PubMed: 12937281]
- Preston LC, Lipscomb S, Robinson P, Mogensen J, McKenna WJ, Watkins H, Ashley CC, Redwood CS. Functional effects of the DCM mutant Gly159Asp troponin C in skinned muscle fibres. *Pflugers Arch* 2007;453:771–776. [PubMed: 17021793]
- Pringle JWS. Stretch activation of muscle: function and mechanism. *Proc R Soc Lond B* 1978;201:107–130. [PubMed: 27795]
- Ranatunga KW. Effects of inorganic phosphate on endothermic force generation in muscle. *Proc Biol Sci* 1999;266:1381–1385. [PubMed: 10445293]
- Rayment I, Rypniewski WR, Schmidt-Bäse K, Smith R, Tomchick DR, Benning MM, Winkelmann DA, Wesenberg G, Holden HM. Three-dimensional structure of myosin subfragment-1: a molecular motor. *Science* 1993;261:50–58. [PubMed: 8316857]
- Regnier M, Morris C, Homsher E. Regulation of the cross-bridge transition from a weakly to strongly bound state in skinned rabbit muscle fibers. *Am J Physiol* 1995;269(6 Pt 1):C1532–C1539. [PubMed: 8572183]
- Rosenfeld SS, Xing J, Whitaker M, Cheung HC, Brown F, Wells A, Milligan RA, Sweeney HL. Kinetic and spectroscopic evidence for three actomyosin: ADP states in smooth muscle. *J Biol Chem* 2001;275:25418–25426. [PubMed: 10827085]
- Saeki Y, Kawai M, Zhao Y. Comparison of crossbridge dynamics between intact and skinned myocardium from ferret right ventricles. *Circ Res* 1991;68:772–781. [PubMed: 1742866]
- Saeki Y, Sagawa K, Suga H. Dynamic stiffness of cat heart muscle in Ba²⁺-induced contracture. *Circ Res* 1978;42:324–333. [PubMed: 624137]
- Sleep JA, Hutton RL. Exchange between inorganic phosphate and adenosine 5'-triphosphate in the medium by actomyosin subfragment 1. *Biochemistry* 1980;19:1276–1283. [PubMed: 6892994]
- Smith DA. A strain-dependent ratchet model for [phosphate]- and [ATP]-dependent muscle contraction. *J Muscle Res Cell Motil* 1998;19:189–211. [PubMed: 9536445]
- Smith DA, Geeves MA. Strain-dependent cross-bridge cycle for muscle. *Biophys J* 1995;69:524–537. [PubMed: 8527667]
- Spirito P, Seidman CE, McKenna WJ, Maron BJ. The management of hypertrophic cardiomyopathy. *N Engl J Med* 1997;336:775–785. [PubMed: 9052657]
- Squire JM, Luther PK, Knupp C. Structural evidence for the interaction of C-protein (MyBP-C) with actin and sequence identification of a possible actin-binding domain. *J Mol Biol* 2003;331:713–724. [PubMed: 12899839]
- Stehle R, Krüger M, Scherer P, Brixius K, Schwinger RH, Pfitzer G. Isometric force kinetics upon rapid activation and relaxation of mouse, guinea pig and human heart muscle studied on the subcellular myofibrillar level. *Basic Res Cardiol* 2002;97(Suppl 1):I127–I135. [PubMed: 12479246]
- Steiger GJ, Abbott RH. Biochemical interpretation of tension transients produced by a four-state mechanical model. *J Muscle Res Cell Motil* 1981;2:245–260. [PubMed: 6457057]
- Stein LA, Greene LE, Chock PB, Eisenberg E. Rate-limiting step in the actomyosin adenosinetriphosphatase cycle: studies with myosin subfragment 1 cross-linked to actin. *Biochemistry* 1985;24:1357–1363. [PubMed: 3157401]
- Swank DM, Vishnudas VK, Maughan DW. An exceptionally fast actomyosin reaction powers insect flight muscle. *Proc Natl Acad Sci USA* 2006;103:17543–17547. [PubMed: 17085600]

- Takagi Y, Shuman H, Goldman YE. Coupling between phosphate release and force generation in muscle actomyosin. *Philos Trans R Soc Lond B Biol Sci* 2004;359:1913–1920. [PubMed: 15647167]
- Tanner BC, Daniel TL, Regnier M. Sarcomere lattice geometry influences cooperative myosin binding in muscle. *PLoS Comput Biol* 2007;3:1195–1211.
- Tawada K, Kawai M. Covalent cross-linking of single muscle fibers from rabbit psoas increases oscillatory power. *Biophys J* 1990;57:643–647. [PubMed: 2306508]
- Taylor EW. Mechanism of actomyosin ATPase and the problem of muscle contraction. *CRC Crit Rev Biochem* 1979;6:103–164. [PubMed: 156624]
- Tesi C, Colomo F, Nencini S, Piroddi N, Poggese C. The effect of inorganic phosphate on force generation in single myofibrils from rabbit skeletal muscle. *Biophys J* 2000;78:3081–3092. [PubMed: 10827985]
- Tesi C, Colomo F, Piroddi N, Poggese C. Characterization of the cross-bridge force-generating step using inorganic phosphate and BDM in myofibrils from rabbit skeletal muscles. *J Physiol* 2002;541(1): 189–199.
- Thirlwell H, Sleep JA, Ferenczi MA. Inhibition of unloaded shortening velocity in permeabilized muscle fibres by caged ATP compounds. *J Muscle Res Cell Motil* 1995;16:131–137. [PubMed: 7622628]
- Thorson J, White DC. Distributed representations for actinmyosin interaction in the oscillatory contraction of muscle. *Biophys J* 1969;9:360–390. [PubMed: 5780714]
- Thorson J, White DC. Role of cross-bridge distortion in the small-signal mechanical dynamics of insect and rabbit striated muscle. *J Physiol* 1983;343:59–84. [PubMed: 6685767]
- Tikunov BA, Sweeney HL, Rome LC. Quantitative electrophoretic analysis of myosin heavy chains in single muscle fibers. *J Appl Physiol* 2000;90:1927–1935. [PubMed: 11299287]
- Vale RD, Oosawa F. Protein motors and Maxwell's demons: does mechanochemical transduction involve a thermal ratchet? *Adv Biophys* 1990;26:97–134. [PubMed: 2150583]
- Wakabayashi K, Sugimoto Y, Tanaka H, Ueno Y, Takezawa Y, Amemiya Y. X-ray diffraction evidence for the extensibility of actin and myosin filaments during muscle contraction. *Biophys J* 1994;67:2422–2435. [PubMed: 7779179]
- Walker JW, Lu Z, Moss RL. Effects of Ca^{2+} on the kinetics of phosphate release in skeletal muscle. *J Biol Chem* 1992;267:2459–2466. [PubMed: 1733945]
- Wang G, Kawai M. Effects of MgATP and MgADP on the cross-bridge kinetics of rabbit soleus slow-twitch muscle fibers. *Biophys J* 1996;71:1450–1461. [PubMed: 8874019]
- Wang G, Kawai M. Force generation and phosphate release steps in skinned rabbit soleus slow-twitch muscle fibers. *Biophys J* 1997;73:878–894. [PubMed: 9251805]
- Wang G, Ding W, Kawai M. Does thin filament compliance diminish the cross-bridge kinetics? A study in rabbit psoas fibers. *Biophys J* 1999;76:978–984. [PubMed: 9916028]
- Wannenburg T, Heijne GH, Geerdink JH, Van Den Dool HW, Janssen PM, De Tombe PP. Cross-bridge kinetics in rat myocardium: effect of sarcomere length and calcium activation. *Am J Physiol* 2000;279:H779–H790.
- Webb MR, Hibberd MG, Goldman YE, Trentham DR. Oxygen exchange between P_i in the medium and water during ATP hydrolysis mediated by skinned fibers from rabbit skeletal muscle: evidence for P_i binding to a force-generating state. *J Biol Chem* 1986;261:15557–15564. [PubMed: 2946675]
- White DC. The elasticity of relaxed insect fibrillar flight muscle. *J Physiol* 1983;343:31–57. [PubMed: 6557139]
- White HD, Taylor EW. Energetics and mechanism of actomyosin adenosine triphosphatase. *Biochemistry* 1976;15:5818–5826. [PubMed: 12793]
- Woledge, RC.; Curtin, NA.; Homsher, E. Energetic aspects of muscle contraction (Monographs of the Physiological Society, No. 41). Academic Press; New York: 1985.
- Xu S, Offer G, Gu J, White HD, Yu LC. Temperature and ligand dependence of conformation and helical order in myosin filaments. *Biochemistry* 2003;42:390–401. [PubMed: 12525166]
- Yates LD, Greaser ML. Quantitative determination of myosin and actin in rabbit skeletal muscle. *J Mol Biol* 1983;168:123–141. [PubMed: 6876172]
- Yount RG, Lawson D, Rayment I. Is myosin a “back door” enzyme? *Biophys J* 1995;68:44S–47S. [PubMed: 7787099]

- Zhao Y, Kawai M. The effect of the lattice spacing change on cross-bridge kinetics in chemically skinned rabbit psoas muscle fibers. II. Elementary steps affected by the spacing change. *Biophys J* 1993;64:197–210. [PubMed: 7679297]
- Zhao Y, Kawai M. Kinetic and thermodynamic studies of the cross-bridge cycle in rabbit psoas muscle fibers. *Biophys J* 1994;67:1655–1668. [PubMed: 7819497]
- Zhao Y, Kawai M. Inotropic agent EMD 53998 weakens nucleotide and phosphate binding to cross bridges in porcine myocardium. *Am J Physiol* 1996;271Heart Circ Physiol 40:H1394–H1406.
- Zhao Y, Swamy PMG, Humphries KA, Kawai M. The effect of partial extraction of troponin C on the elementary steps of the cross-bridge cycle in rabbit psoas fibers. *Biophys J* 1996;71:2759–2773. [PubMed: 8913613]

Appendix 1

The solution of the differential equation (A1) can be found in the following way.

$$dY(t)/dt + \lambda Y(t) = h \quad (\text{A1})$$

Now we substitute $Y(t)$ with $Z(t)$ so that

$$Y(t) \equiv h/\lambda + Z(t)\exp(-\lambda t) \quad (\text{A2})$$

is satisfied. From Eq. A2,

$$dY(t)/dt = [-\lambda Z(t) + dZ(t)/dt]\exp(-\lambda t) \quad (\text{A3})$$

By substituting Eqs. A2 and A3 to Eq. A1, we arrive at

$$dZ(t)/dt = 0 \quad (\text{A4})$$

By integrating Eq. A4, we get

$$Z(t) = Y_0 \quad (\text{A5})$$

where Y_0 is the integration constant. From Eqs. A2 and A5, we get

$$Y(t) = Y_0 \exp(-\lambda t) + h/\lambda \quad (\text{A6})$$

Therefore, Eq. A1 has an exponential process with the rate constant λ , amplitude Y_0 , and the steady state value h/λ (Eq. A6). Y_0 is determined by the initial conditions.

Appendix 2

In Scheme 3, the following differential equations can be set up.

$$dA/dt = -(\alpha + \gamma')A + \alpha' B + \gamma C \quad (\text{A7})$$

$$dB/dt = \alpha A - (\beta + \alpha')B + \beta' C \quad (\text{A8})$$

$$dC/dt = \gamma' A + \beta B - (\gamma + \beta')C \quad (\text{A9})$$

Eqs. A7–A9 can be written in matrix form.

$$\frac{dX}{dt} = -HX \quad (\text{A10})$$

$$\text{where } X(t) \equiv \begin{pmatrix} A(t) \\ B(t) \\ C(t) \end{pmatrix} \quad (\text{A11})$$

$$\text{And } H \equiv \begin{pmatrix} (\alpha + \gamma') & -\alpha' & -\gamma \\ -\alpha & (\beta + \alpha') & -\beta' \\ -\gamma' & -\beta & (\gamma + \beta') \end{pmatrix} \quad (\text{A12})$$

$$\text{Also, } A = B + C = A_T \quad (\text{A13})$$

Note the similarity of Eqs. A1 and A10. Note also that $|H| = \det(H) = 0$, which is consistent with Eq. A13. The eigen values (λ) of matrix H can be found by determining the roots of Eq. A14.

$$|H - I\lambda| = \begin{vmatrix} (\alpha + \gamma') - \lambda & -\alpha' & -\gamma \\ -\alpha & (\beta + \alpha') - \lambda & -\beta' \\ -\gamma' & -\beta & (\gamma + \beta') - \lambda \end{vmatrix} = 0 \quad (\text{A14})$$

where I is the identity matrix. From Eq. A14,

$$\lambda^3 - 2Q\lambda^2 + M\lambda = 0 \quad (\text{A15})$$

$$\text{where } Q \equiv (\alpha + \alpha' + \beta + \beta' + \gamma + \gamma')/2$$

and

$$M \equiv \alpha\beta + \beta\gamma + \gamma\alpha + \alpha\beta' + \beta\gamma' + \gamma\alpha' + \alpha'\beta' + \beta'\gamma' + \gamma'\alpha' \quad (\text{A16})$$

Equation A15 has three roots λ_1 , λ_2 , and λ_3 .

$$\lambda_1 = 0$$

$$\lambda_2 = Q + \sqrt{R} \quad (\text{A17})$$

$$\lambda_3 = Q - \sqrt{R} = \frac{M}{Q + \sqrt{R}} \quad (\text{A18})$$

$$\text{where } R \equiv Q^2 - M$$

where $R \equiv Q^2 - M$

With Eqs. A17 and A18, Eq. A10 can be solved to result in:

$$X(t) = UE(t) \quad (\text{A19})$$

$$\text{where } U \equiv \begin{pmatrix} A_1 & U_{12} & U_{13} \\ B_1 & U_{22} & U_{23} \\ C_1 & U_{32} & U_{33} \end{pmatrix}, \quad \text{and} \\ E(t) \equiv \begin{pmatrix} 1 \\ \exp(-\lambda_2 t) \\ \exp(-\lambda_3 t) \end{pmatrix} \quad (\text{A20})$$

The elements U_{i2} and U_{i3} ($i = 1, 2, 3$) are 2 eigen vectors (column vectors) of matrix H (Eq. A12) corresponding to λ_2 and λ_3 , respectively, and they are time-independent variables. Their size (length) is determined by the initial conditions (2 independent variables). A_1 , B_1 and C_1 are the steady-state concentrations (see below). The correctness of Eq. A19 can be examined by substituting it into Eq. A10 keeping in mind that:

$$U^{-1}HU = \begin{pmatrix} \lambda_1 & 0 & 0 \\ 0 & \lambda_2 & 0 \\ 0 & 0 & \lambda_3 \end{pmatrix}$$

From Eqs. A19 and A20, the individual solutions are:

$$A(t) = A_1 + U_{12}\exp(-\lambda_2 t) + U_{13}\exp(-\lambda_3 t) \quad (\text{A21})$$

$$B(t) = B_1 + U_{22}\exp(-\lambda_2 t) + U_{23}\exp(-\lambda_3 t) \quad (\text{A22})$$

$$C(t) = C_1 + U_{32}\exp(-\lambda_2 t) + U_{33}\exp(-\lambda_3 t) \quad (\text{A23})$$

Therefore, according to Eq. 34, a force transient has two exponential processes that correspond to phases 2 and 3, with the rate constants λ_2 and λ_3 , respectively.

If $R < 0$, then λ_2 , λ_3 , U_{12} and U_{13} are complex numbers, and $\lambda_3 = \lambda_2^*$ (Eqs. A17 and A18), and $U_{13} = U_{12}^*$, where * indicates the complex conjugate. In this case, Eq. A19 can be rearranged to result:

$$X(t) = \begin{pmatrix} A_1 & 2\Re(U_{12}) & 2\Im(U_{12}) \\ B_1 & 2\Re(U_{22}) & 2\Im(U_{22}) \\ C_1 & 2\Re(U_{32}) & 2\Im(U_{32}) \end{pmatrix} \begin{pmatrix} 1 \\ \exp(-Qt)\cos\sqrt{-R} \cdot t \\ \exp(-Qt)\sin\sqrt{-R} \cdot t \end{pmatrix} \quad (\text{A24})$$

where $\Re(U_{ij})$ refers to the real, and $\Im(U_{ij})$ to the imaginary part of the complex number U_{ij} . Equation A24 shows that this system has a damped oscillation. However, in literature dealing with muscle fibers, it is rare to find force transients with a damped oscillation in response to a sudden change in an experimental condition. If a force transient should oscillate, a resonance of the force transducer should be suspected before a conclusion is drawn. The fact that an oscillation is absent implies that the intrinsic rate constants among the three steps in Scheme 3 differ significantly.

Steady state

By setting $dA/dt = 0$ and $dB/dt = 0$ in Eqs. A7 and A8, and with the constraints of Eq. A13, we can solve the steady-state concentrations of A_1 , B_1 and C_1 . These three values constitute an eigen vector (column vector) which belongs to the eigen value λ_1 M is defined in Eq. A16.

$$A_1 = A_t (\beta\gamma + \gamma\alpha' + \alpha'\beta') / M \quad (\text{A25})$$

$$B_1 = A_t (\gamma\alpha + \alpha\beta' + \beta'\gamma') / M \quad (\text{A26})$$

$$C_1 = A_T(\alpha\beta + \beta\gamma' + \gamma'\alpha')/M \quad (\text{A27})$$

The turnover (ATP hydrolysis) rate is:

$$\begin{aligned} J &= \alpha A_1 - \alpha' B_1 = \beta B_1 - \beta' C_1 = \gamma C_1 - \gamma' A_1 \\ &= A_T(\alpha\beta\gamma - \alpha'\beta'\gamma')/M \end{aligned} \quad (\text{A28})$$

A similar analysis based on Scheme 8 is found in the Appendix of Kawai (2003).

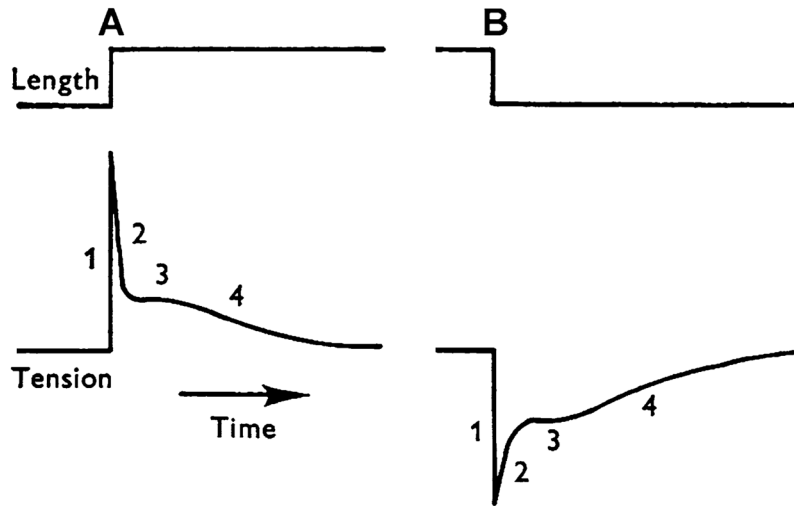


Fig. 1.
 A sketch of stretch (at A) and release (at B) experiments during a plateau of active tension in frog semitendinosus fibers. Four phases of tension transients are indicated. Modified from Fig. 1 of Heintz et al. (1974) and reproduced with permission from *The Journal of Physiology* (London)

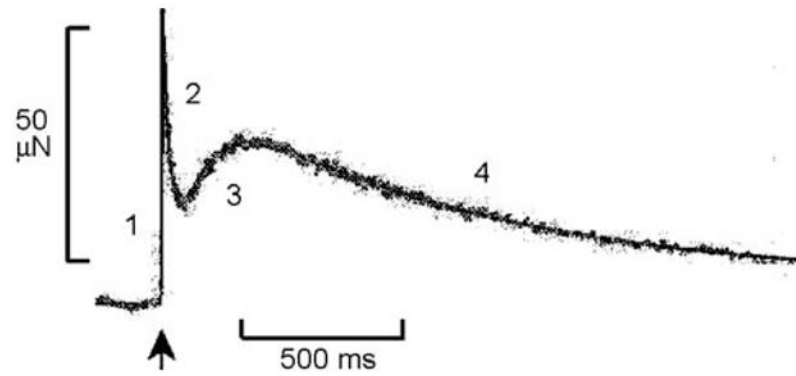


Fig. 2. A record of the force time course that occurs in response to a step-length increase (at ↑, 1.5 nm/half sarcomere, which is about 0.12%) in rabbit psoas fibers at 5°C during Ca²⁺ activation. Numbers indicate four phases of tension transients. Modified from Fig. 3 of Davis et al. (2002), and reproduced with permission from the Biophysical Society

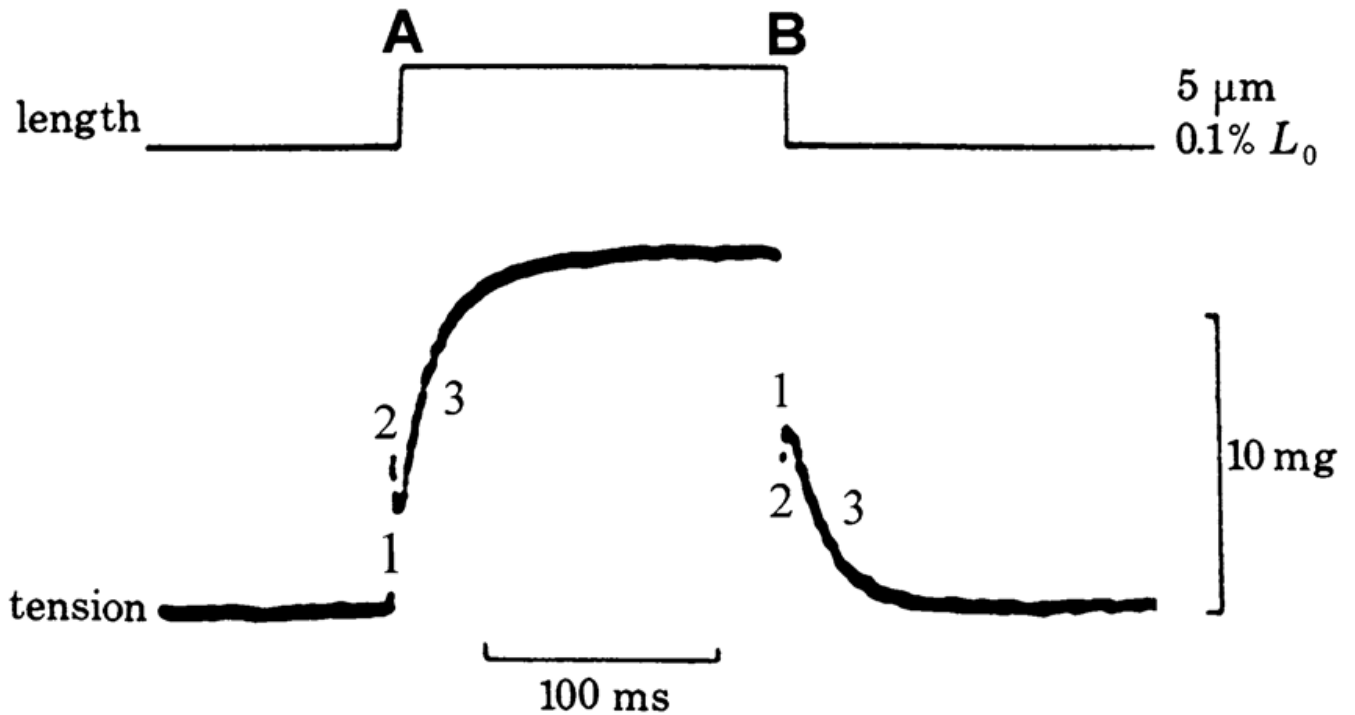


Fig. 3.

A record of the force time course that occurs in response to a step-length increase (0.1%) (at A) and the ensuing decrease (at B), in insect fibrillar muscle fibers. Three phases of the tension transient are indicated. Phase 3 is most prominent in this muscle preparation, and is known as “delayed rise in tension” on stretch, and as “delayed fall in tension” on release. 10 mg force = 98 μN . Modified from Fig. 5a of Pringle (1978), the original data having been generated by Roger H. Abbott. Reproduced with permission from the Royal Society (London)

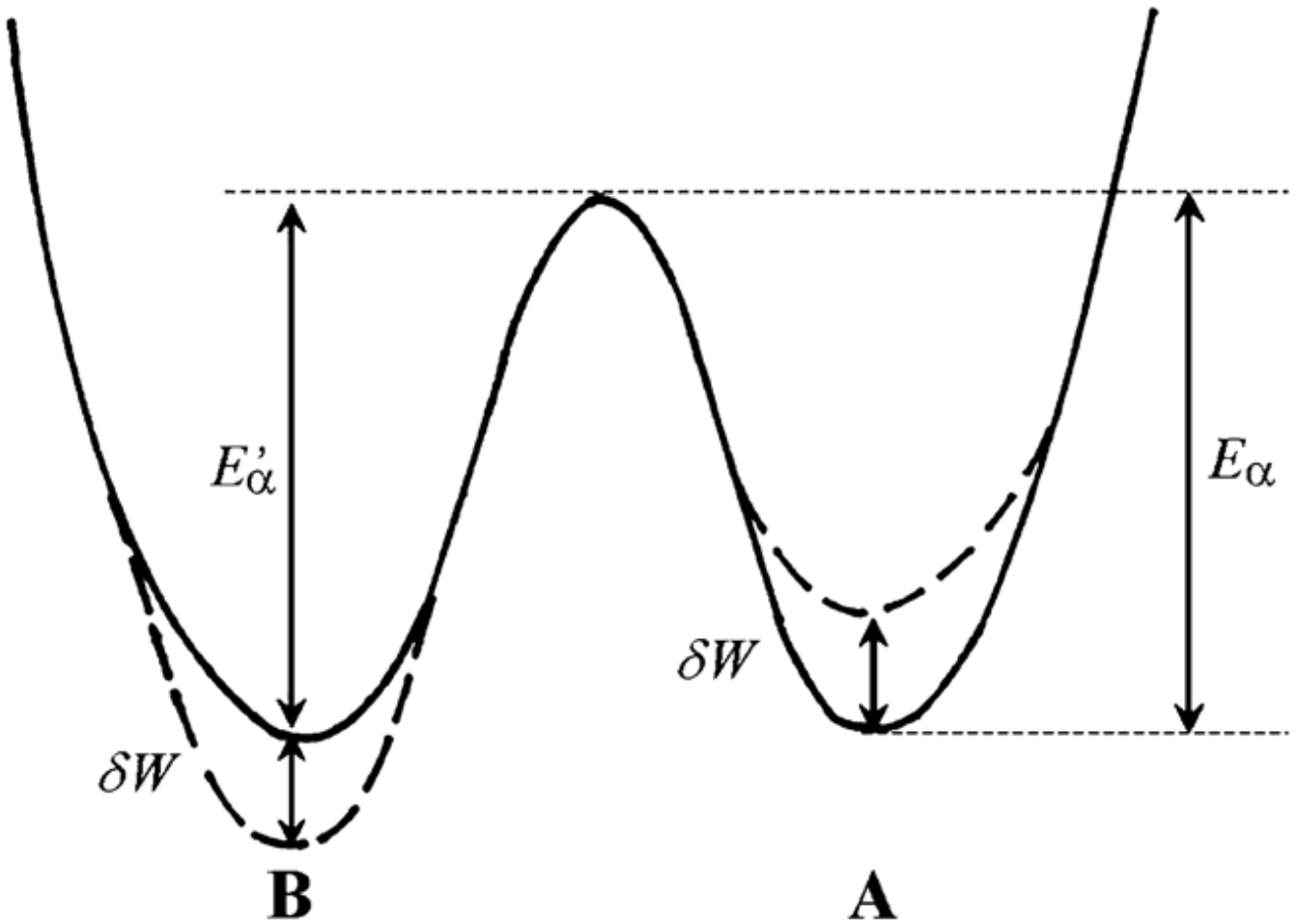


Fig. 4. The reaction profile of Scheme 1 with stretch ($\delta l > 0$) that either (1) decreases the activation energy (E_α) of force-generating state **A** by δW , or (2) increases the activation energy (E'_α) of the detached state **B** by δW , where $\delta W = \varphi \delta l$, and φ is unitary force (force/cross-bridge). From this it follows that $\delta E_\alpha = -\delta W = -\varphi \delta l$ and/or $\delta E'_\alpha = +\delta W = \varphi \delta l$. All equations are the same for release, except that $\delta l < 0$

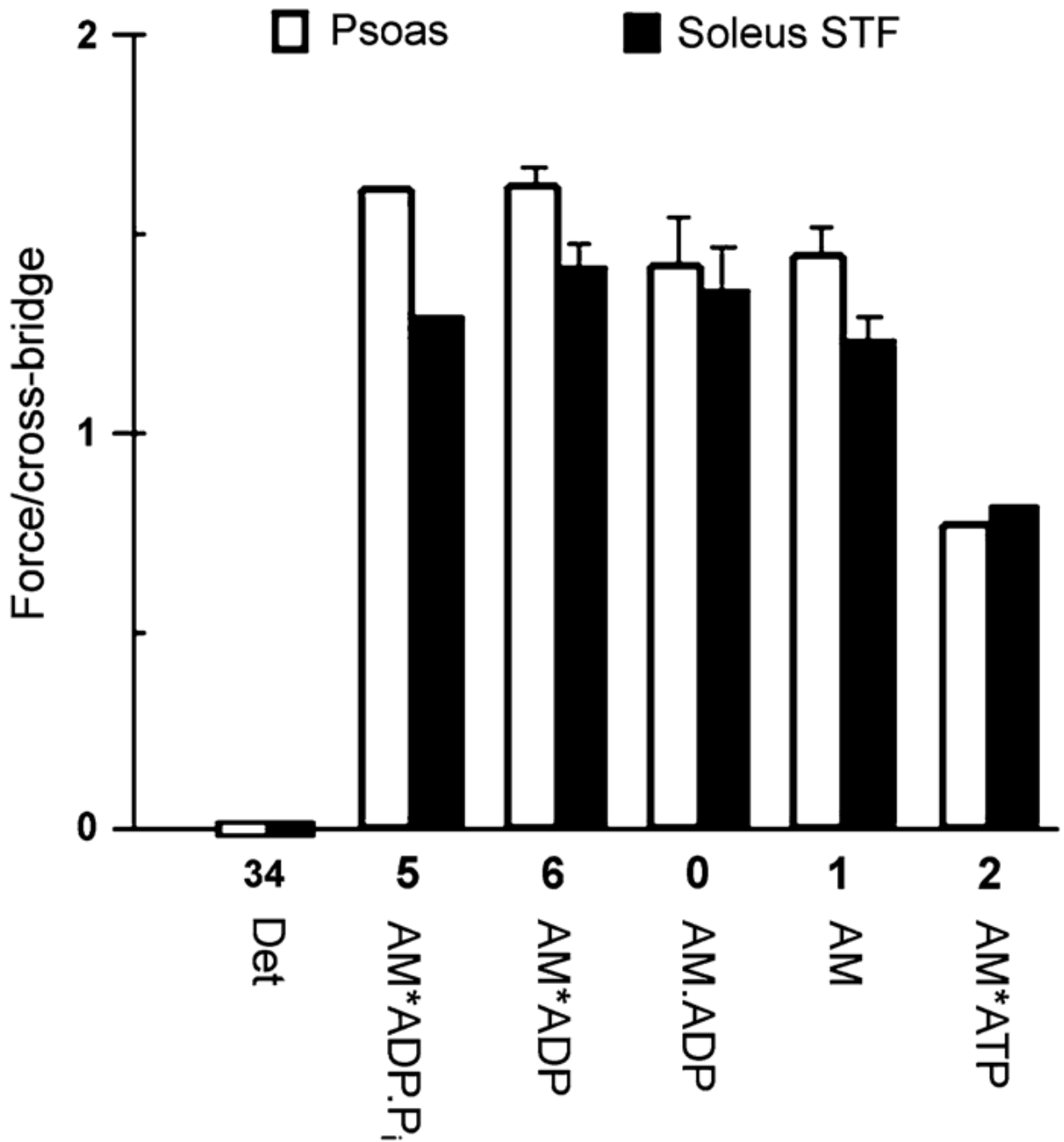


Fig. 5.

Force generated (or supported) by each cross-bridge state. □ Rabbit psoas fibers (replotted from Kawai and Zhao 1993). ■ Rabbit soleus slow twitch fibers (plotted from data published by Wang and Kawai 1997). The data are normalized to the force generated in response to standard activation (T_C), which is a mixture of all states. The **Det** state includes both weakly attached states (AM.ATP, AM.ADP.Pi) and truly detached states (M.ATP, M.ADP.Pi). Error bars represent SEM

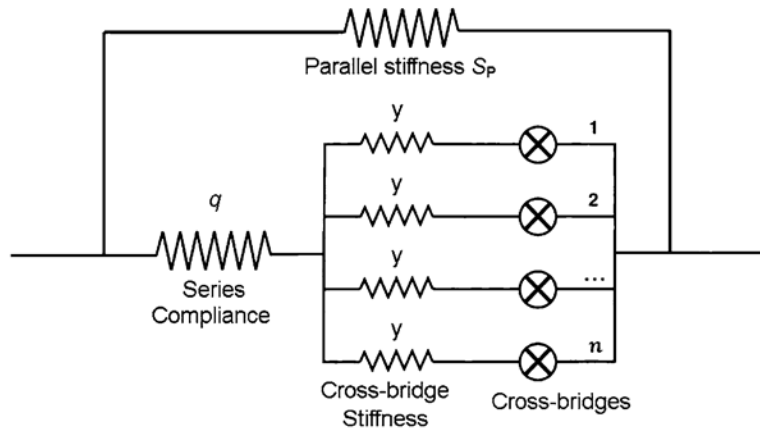
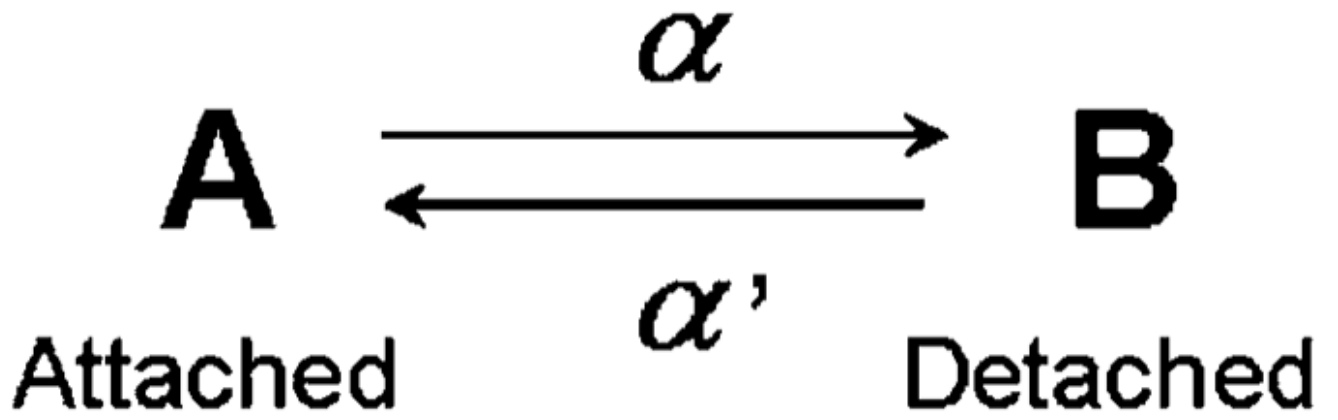
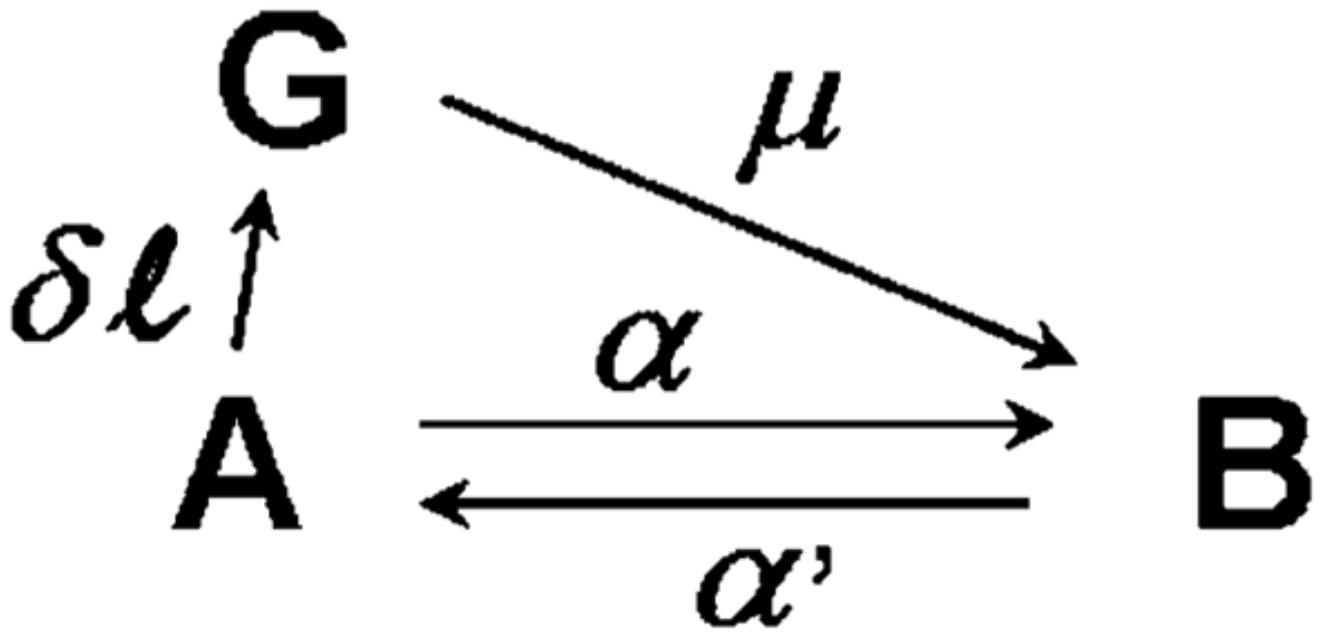


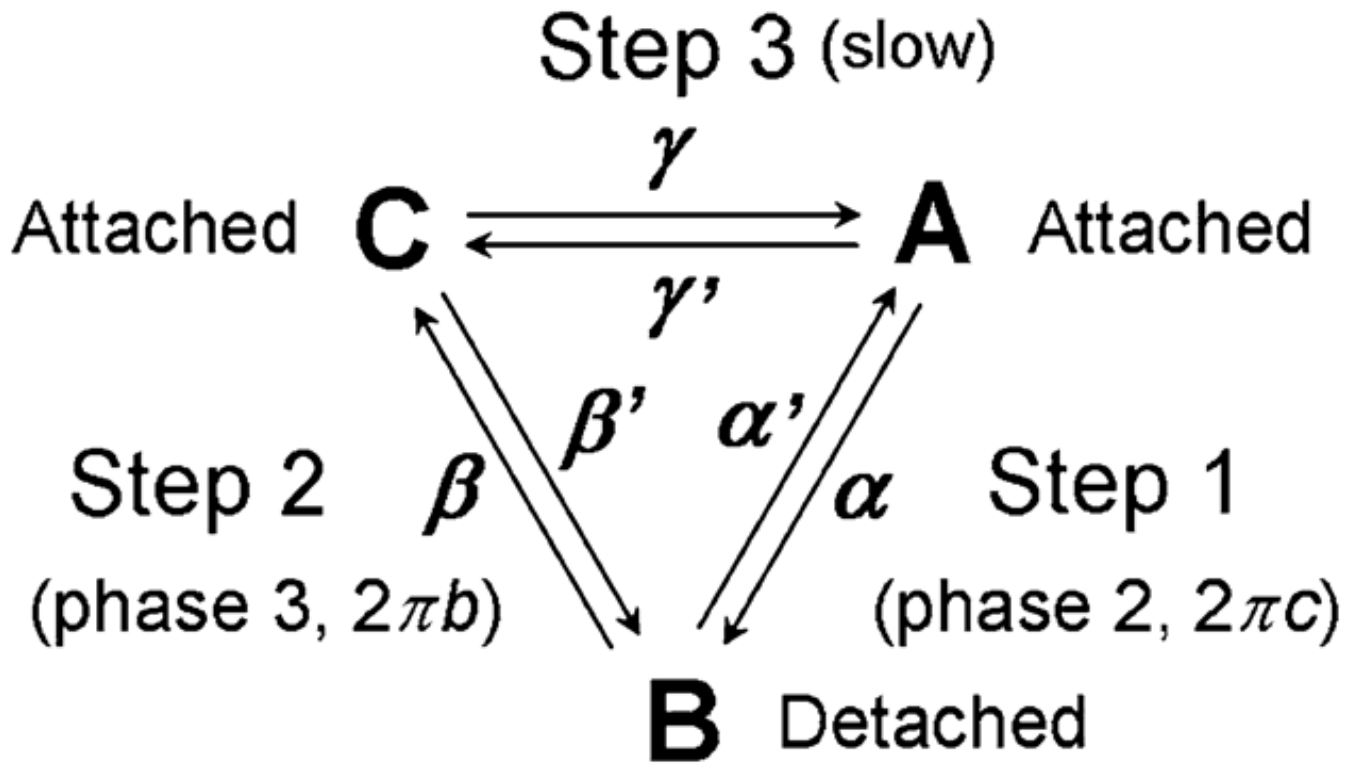
Fig. 6. A mechanical equivalent of one half sarcomere. Cross-bridges are arranged in parallel, and this assembly is connected to a series compliance (q). The parallel stiffness (S_p) is added to the entire structure. Although each element is written as elastic, each can have a viscous property at the same time. Modified from Fig. 9 of Wang and Kawai (1997), and reproduced with permission from the Biophysical Society



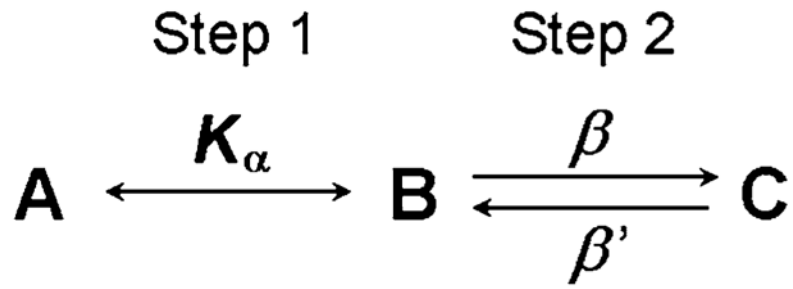
Scheme 1.
The two-state model



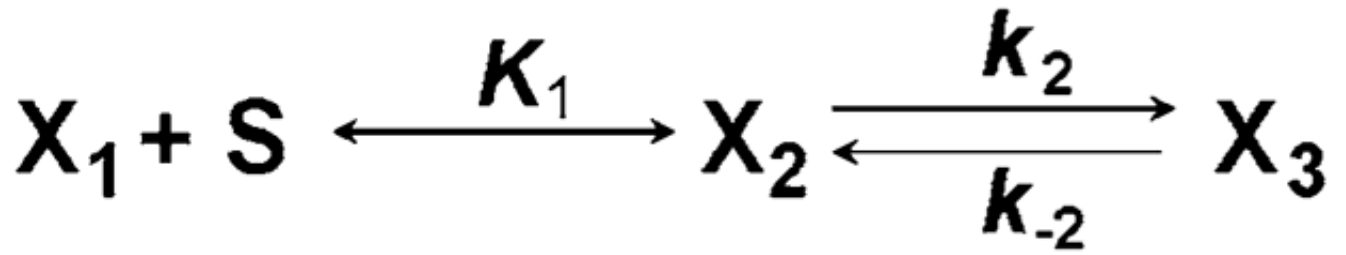
Scheme 2.
The expanded two-state model



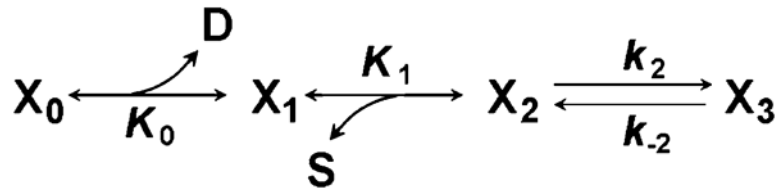
Scheme 3.
The three-state model

**Scheme 4.**

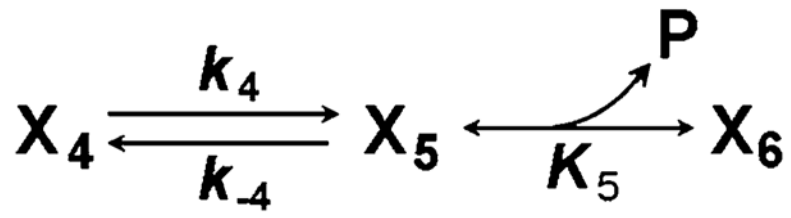
The medium-speed approximation of the three-state model

**Scheme 5.**

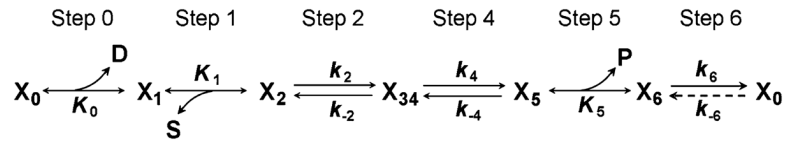
The model representing ATP (S) binding and the conformational change

**Scheme 6.**

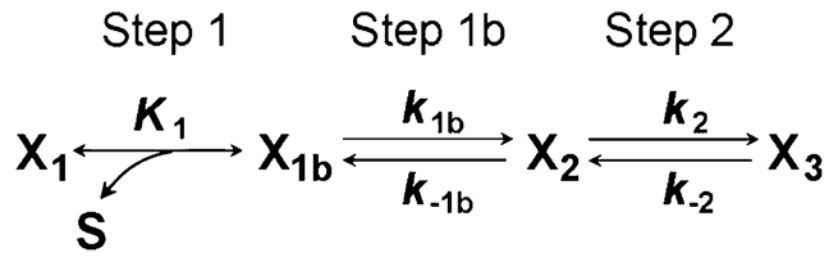
The model showing ADP (D) as a competitive inhibitor of ATP



Scheme 7.
The two-step mechanism of phosphate (P) release



Scheme 8.
The combined cross-bridge model with six states

**Scheme 9.**

An additional step (step 1b) to account for process D

Table 1

Mathematical symbols used; (*t*) indicates time-dependent variable; Sch = Scheme

Symbol	Section	Definition
$A(t)$	2	Concentration of cross-bridges in A
A_1	2	Steady-state concentration of A
A_C	5	Cross-sectional area
A_T	2, 18	Total concentration of myosin S1
α	2, 6	Rate constant of detachment (A → B), Sch 1–3
α'	2, 6	Rate constant of attachment (B → A), Sch 1–3
$B(t)$	2, 6	Concentration of detached cross-bridges
B_1	2	Steady-state concentration of B β 6 Rate constant of attachment (B → C), Sch 3
β'	6	Rate constant of detachment (C → B), Sch 3
$C(t)$	6	Concentration of attached cross-bridges in C
C_1	6	Steady-state concentration of C D 12 MgADP concentration
$\delta, \delta x$	3	Perturbation
δl	4	Stretch applied to a cross-bridge ($\delta l > 0$). $\delta l < 0$ for release
δW	4	Work performed on a cross-bridge by stretch ($\delta W > 0$). $\delta W < 0$ for release. Eq. 16
E_α	4	Activation energy of α (A → B), Fig. 4A
$E_{\alpha'}$	4	Activation energy of α' (B → A), Fig. 4B
ε	12	$\varepsilon \equiv K_1 S / (1 + K_0 D + K_1 S)$, Eq. 49
η	19	Step size
$F(t)$	5	Force time course
F_0	19	Isometric force at steady state
$F_A(t)$	5	Force contribution by state A
$F_G(t)$	5	Force contribution by state G
ϕ	4, 9	Unitary force, force/cross-bridge
$G(t)$	5	Concentration of strained cross-bridges, Sch 2
G_1	5	Steady-state concentration of G
γ	6	Rate constant of C → A , Sch 3
γ'	6	Rate constant of A → C , Sch 3
H	A2	Reaction matrix, Eq. A12
J	8, 18	Turnover rate (ATPase), Eqs. 40, 58
K_0	12	Association constant of MgADP, Sch 6
K_1	11	Association constant of MgATP, Sch 5
k_{1b}	16	Rate constant of step 1b, Sch 9
k_{-1b}	16	Reversal rate constant of step 1b, Sch 9
k_2	11	Rate constant of step 2, Sch 5
k_{-2}	11	Reversal rate constant of step 2, Sch 5
K_2	12	Equilibrium constant of step 2, $K_2 \equiv k_2/k_{-2}$
k_4	13	Rate constant of step 4, Sch 7

Symbol	Section	Definition
k_{-4}	13	Reversal rate constant of step 4, Sch 7
K_4	15	Equilibrium constant of step 4, $K_4 \equiv k_4/k_{-4}$
K_5	13	Association constant of Pi, Sch 7
k_6	14, 18	Rate constant of step 6, Sch 8
k_{-6}	14	Reversal rate constant of step 6, Sch 8
K_6	14	Equilibrium constant of step 6, $K_6 \equiv k_6/k_{-6}$
K_α	7	Equilibrium constant of $\mathbf{A} \leftrightarrow \mathbf{B}$. $K_\alpha \equiv \alpha/\alpha'$
K_β	7	Equilibrium constant of $\mathbf{B} \leftrightarrow \mathbf{C}$. $K_\beta \equiv \beta/\beta'$
k_B	4	Boltzmann's constant, $k_B = 1.381 \times 10^{-23} \text{ JK}^{-1}$
l_0	5	Half sarcomere length
λ	2	Apparent rate constant, $\lambda \equiv \alpha + \alpha'$, Eq. 4
λ_2	7, 11	Apparent rate constant of phase 2. $\lambda_2 = 2\pi c$. Eqs. 32, 44, 50
λ_3	7, 13	Apparent rate constant of phase 3. $\lambda_3 = 2\pi b$. Eqs. 37, 53, 54
λ_4	19	Rate constant of force development, Eq. 63
M	8, A2	Eqs. 39, A16
μ	5	Perturbed rate constant α by stretch δl . $\mu \equiv \alpha + \delta\alpha$
N_A	5	Avogadro's number, $N_A = 6.022 \times 10^{23}/\text{mole}$
ν	19	Number of cross-bridge cycles in 1 sec
P	13	Phosphate concentration
$2\pi a$	19	Rate constant of process A (phase 4)
$2\pi b$	10	Rate constant of process B (phase 3)
$2\pi c$	10	Rate constant of process C (phase 2)
q	17	Series compliance of half sarcomere
R	15	Gas constant, $R = k_B N_A = 8.314 \text{ JK}^{-1}\text{mol}^{-1}$
ρ	5	Cross-bridge stiffness
ρ'	19	Stiffness of half sarcomere
S	11	Substrate (MgATP) concentration
σ	12	$\sigma \equiv K_1 S K_2 / [1 + K_0 D + K_1 S (1 + K_2)]$, Eq. 52
S_p	17	Parallel stiffness of half sarcomere
t	2	Time
T	4	Absolute temperature
T_0	15	Tension supported by \mathbf{X}_0 (AM.ADP)
T_1	15	Tension supported by \mathbf{X}_1 (AM), Eq. 55
T_{1b}	15	Tension supported by \mathbf{X}_{1b} (AM [†] ATP)
T_2	15	Tension supported by \mathbf{X}_2 (AM*ATP), Eq. 55
T_{34}	15	Tension supported by \mathbf{X}_{34} (Det), $T_{34} = 0$
T_5	15	Tension generated/supported by \mathbf{X}_5 (AM*ADP.P)
T_6	15	Tension generated/supported by \mathbf{X}_6 (AM*ADP)
T_C	15	Tension of standard activation, C=control
U	A2	3×3 eigen matrix consisting of 3 eigen (column) vectors. Eq. A20

Symbol	Section	Definition
$X_0(t)$	12	Probability of cross-bridges at AM.ADP
$X_1(t)$	11	Probability of cross-bridges at AM
$X_{1b}(t)$	11	Probability of cross-bridges at AM [†] ATP
$X_2(t)$	11	Probability of cross-bridges at AM*ATP
$X_{34}(t)$	14	Probability of cross-bridges at Det state
$X_5(t)$	13	Probability of cross-bridges at AM*ADP.Pi
$X_6(t)$	13	Probability of cross-bridges at AM*ADP
$X_a(t)$	12	Probability of strongly attached cross-bridges, Eq. 57, $X_a \equiv X_0 + X_1 + X_2 + X_5 + X_6$
Y_a	17	Stiffness of cross-bridges in half sarcomere when all are strongly attached
ζ	21	$\zeta \equiv K_5P/(1 + K_5P)$, Eq. 73

Table 2

Kinetic constants of the cross-bridge cycle of Scheme 8

Animal and muscle	K_0 , mM ⁻¹	K_1 , mM ⁻¹	k_{1b} , s ⁻¹	k_{1a} , s ⁻¹	k_{2} , s ⁻¹	k_{-2} , s ⁻¹	k_4 , s ⁻¹	k_{-4} , s ⁻¹	K_S , mM ⁻¹	Perturbation	Source
Rabbit psoas	2.8	1.4	1530 ^a	1610 ^a	440	100	56	129	0.069	Length	Kawai and Halvorson (1991)
Rabbit psoas	-	-	-	-	-	-	79.2	114.7	0.27	Pi	Dantzig et al. (1992)
Rabbit psoas, 15°C	-	-	-	-	-	-	27	115	0.164	Pi	Walker et al. (1992)
Rabbit psoas, 12°C	-	-	-	-	-	-	~15 ^b	~36 ^b	0.255	Pressure	Fortune et al. (1991)
Rabbit AM, type IIB	5	0.84	-	-	526	328	143	81	0.26	Length	Galler et al. (2005)
Rabbit AM, type IID	18	4.9	-	-	352	121	58	63	0.16	Length	Galler et al. (2005)
Rabbit EDL and soleus, type IIA	-	8.7	-	-	198	51	13.6	13.6	0.18	Length	Galler et al. (2005)
<i>Drosophila melanogaster</i> , indirect flight, 15°C	-	0.19	-	-	3698	8	1778	11	-	Length	Swank et al. (2006)
<i>Lethocerus colossicus</i> , indirect flight	-	0.7	-	-	900	180	-	150 ^c	0.13 ^c	Length	Marcussen and Kawai (1990)
Rabbit soleus, type I	18	1.2	90	100	21	14.1	5.7	4.5	0.18	Length	Wang and Kawai (1997)
Ferret cardiac	-	0.99	270	280	48	14	11	107	0.060	Length	Kawai et al. (1993)
Porcine cardiac	80	10.6	-	-	13.0	9.1	3.2	10.5	0.104	Length	Zhao and Kawai (1996)
Bovine cardiac, 25°C	-	9.1	-	-	26.6	12.1	7.1	12.6	0.14	Length	Fujita et al. (2002)

Temperature at 20°C unless otherwise stated. AM = adductor mangus, EDL = extensor digitorum longus. The nomenclature of the kinetic constants is based on Scheme 8 and common units are used. Hence, it does not necessarily reflect the nomenclature used in the original publication. k_1b and k_{-1b} are defined in Scheme 9

^aValues based on Zhao and Kawai (1993)

^bEstimated from Fig. 4A of Fortune et al. (1991) and $k_4 + k_{-4} = 51 \text{ s}^{-1}$ as described in its legend

^cEstimate based on Fig. 8 of Marcussen and Kawai (1990)